Precession, Eccentricity, Obliquity, Insolation and Paleoclimates

Article · January 1994

DOI: 10.1007/978-3-642-79066-9_5

2 authors:

André Berger
Université Catholique de Louvain - UCLouvain
258 PUBLICATIONS **20,493** CITATIONS
SEE PROFILE

Marie-France Loutre
PAGES (Past Global Changes)
176 PUBLICATIONS **15,344** CITATIONS
SEE PROFILE

PRECESSION, ECCENTRICITY, OBLIQUITY, INSOLATION AND PALEOCLIMATES

A. Berger and M.F. Loutre
Université Catholique de Louvain
Institut d'Astronomie et de Géophysique G. Lemaître
2 Chemin du Cyclotron
B-1348 Louvain-la-Neuve, Belgium

Abstract. Different parameters related to the solar radiation received at the top of the atmosphere are derived and their long-term variations analysed in the frequency domain. The annual mean energy received by the whole Earth is varying in time according to the variations of the mean distance from the Earth to the Sun, i.e. as a function of $(1-e^2)^{-\frac{1}{2}}$. The so-called 100 ka period of the eccentricity (and the other periods as well) are originating from a combination of the fundamental periods of the climatic precession parameters. The insolation at a given latitude and for a fixed longitude of the Earth on its orbit is a function of obliquity through the factor related to the zenith angle of the Sun and of precession through the distance factor. Moreover a deeper analysis of the spectrum of the distance factor shows that it contains also, with much less power, half precession periods, eccentricity periods and combination tones between eccentricity and precession. Over the Quaternary, the latitudes of the polar and the tropical circles, varying with obliquity, are situated respectively between 65.5° and 68° and between 22° and 24.5°. Their present-day motion towards north is estimated to be 14.4 m per year. Finally, it is shown that in most insolation parameters, the precessional signal dominates the obliquity one, except in high polar latitudes mainly of the winter hemisphere, although the power of the obliquity signal increases from low to high latitudes.

1 Insolation frequencies in paleoclimatic records

Since the late 1960's, judicious use of radioactive dating and paleomagnetic techniques gradually clarified the Pleistocene time scale (Broecker et al., 1968; Bard et al., 1990). Better instrumental methods came on the scene for determining oxygen isotopes for ice-age foraminifera relics (Emiliani, 1966), ecological methods of core interpretation were perfected (Imbrie and Kipp, 1971), global climates in the past were reconstructed (CLIMAP, 1976, 1981) and atmospheric general circulation models and climate models became available (Kutzbach, 1985; Crowley, 1988; COHMAP members, 1988; Berger et al., 1990; Gallée et al., 1992). With these improvements in dating and interpreting geological data in terms of paleoclimates, with the increased use of computers and the development of astronomical and climate models, a more critical and deeper investigation of the astronomical theory is now possible.

NATO ASI Series, Vol. I 22
Long-Term Climatic Variations
Edited by J.-C. Duplessy and M.-T. Spyridakis

According to the astronomical theory of paleoclimates (Berger, 1988), the perturbations in the Earth's orbital parameters change sufficiently the latitudinal distribution and the seasonal pattern of insolation received at the top of the atmosphere to trigger climate variations at the 10 to 100 ka time scales. The Milankovitch theory (1941) is a particular version of this more general astronomical theory of paleoclimates, Milankovitch using the caloric seasons to explain the long-term climatic variations during the Quaternary.

From spectral analysis of climate sensitive indicators extracted from selected deep-sea records of the southern Indian Ocean, Hays, Imbrie and Shackleton demonstrated for the first time in 1976 that the astronomical frequencies (corresponding to the 100, 41, 23 and 19 ka periods) are significantly superimposed upon a general red noise spectrum. It is the geological observation of the bipartition of the precessional peak (23 and 19 ka were found instead of the usual 21 ka), confirmed in the astronomical computations made independently by Berger (1977a), which was one of the first most delicate and impressive of all tests for the Milankovitch theory. This landmark paper also showed that the 100-ka period contribution to the total variance far exceeds that expected from a simple linear relationship between insolation and ice volume and that there is a fairly consistent phase relationship between insolation, sea surface temperature and ice volume, each preceded the next by 2 to 4 ka.

Since 1976, spectral analysis of climatic records of the past 800 ka or so, has provided substantial evidence that, at least near the frequencies of variation in obliquity and precession, a considerable fraction of the climatic variance is driven in some way by insolation changes accompanying the perturbations of the Earth's orbit (Imbrie and Imbrie, 1980; Imbrie et al., 1984; Imbrie et al., 1989; Berger, 1989a).

However, the shape of the spectrum depends also upon the location of the core and the nature of the climatic parameter analysed (Hays et al., 1976). For example, analysis of geologic time series from the subpolar North Atlantic (Ruddiman and McIntyre, 1984) indicates that SST fluctuations, a monitor of the oceanic polar front, varied with a 41-ka period, a response consistent with a dominant influence by the high latitude tilt signal of the Milankovitch caloric insolation. Farther south, along the latitude of the southern terminus of the Laurentide Ice Sheet (about 45°N), SST varied on a 23-ka period. Milankovitch cycles can also be found in eolian sediments and mid-and high-latitude pollen records. Over the North Pacific, a long time series of eolian transport from interior east-

ern Asia records significant fluctuations at the 100-ka and 41-ka periods. Janecceck and Rea (1984) suggest that this 41-ka period result from tilt variations that cause changes in equator-to-pole temperature gradients (and hence wind). A pollen series from Grande Pile, France (Woillard, 1978), yields spectra dominated by 23-ka precession power, but also with indications of significant higher frequencies (Molfino et al., 1984). A series of analyses indicate that North Atlantic Deep Water also fluctuated at 41-ka periods with NADW lagging obliquity by about 8,000 years (Boyle and Keigwin, 1985/1986).

In low latitudes, climate fluctuations have more 23-ka power on both land and sea. In the Arabian Sea, an upwelling index related to the Asian monsoon has 23 ka fluctuations that lag precession by about 5 000 years (Prell, 1984). An index of African aridity has been developed based on abundances of african freshwater diatoms in equatorial Atlantic sediments which fluctuation have clear 23-ka power (Pokras and Mix, 1987). McIntyre et al. (1989) found very strong 23-ka power in a foraminifera record from the eastern equatorial Atlantic. There is also 41-ka power in this series, a response that may reflect a tilt peak at the equator according to Short et al. (1990).

There is also a growing body of information available as to fluctuations of various components of the carbon cycle. For example, the ice core CO_2 record has significant power in Milankovitch bands especially at 21 ka, although the temperature spectrum indicates periods around 40 and 20 ka, with the 40 ka dominating the 20 ka (Barnola et al., 1987; Jouzel et al., 1987). Shackleton and Pisias (1985) demonstrated that benthic $\delta^{13}C$, a measure of whole-ocean carbon storage, increased in the glacials with the fluctuations coherent and in phase with ice volume changes. Their measures of ocean productivity have significant 23-ka power, although equatorial Atlantic productivity indices measured by Curry and Crowley (1987) have 100-ka and 41-ka signals but no 23-ka power.

In the Mediterranean Pliocene, rhythmic lithological variations in the Trubi and Narbone Formations of Sicily and Calabria show cycles that could be related to precession and eccentricity (Hilgen, 1987). In particular, the precession cycle corresponds well with the mean duration of the deposition of basic rhythmites, which comprise small-scale, bipartite or quadripartite marl rhythms in the Trubi and individual sapropelitic layers in the Narborne Formation. The 100 and 400 ka cycles of eccentricity would match the average duration of both layer-scale marl rhythms in the Trubi, which approximately comprise 5 and 20 basic rhythmites respectively, as well as small-scale and large-scale clusters of

sapropelitic layers in the Narbone Formation. However, consistent discrepancies in the Rossello composite section (Pliocene of Sicily, Hilgen and Langereis, 1989) could argue for an age re-assignment of the Gilbert and Gauss chrons based on phase relations between the sedimentary and supposedly corresponding orbital cycles.

A similar conclusion is shown by Shackleton et al. (1990) who proposed that the currently adopted radiometric dates for the Matuyama-Bruhnes boundary, the Jaramillo and Olduvai Subschrons and the Gauss-Matuyama boundary underestimate their true astronomical age by between 5 and 7 %. The basis for such a revised time scale is the stronger contribution from the precession signal in the record from ODP Site 677.

There is also evidence that the orbital variations were linked to climate at periods shorter than 100 ka during the past few hundred million years (Fischer, 1986; Berger, 1989b). This appeared at times when major ice masses were probably absent. Walsh power spectra of the Blue Lias Formation (basal Jurassic) show two cycles with duration less than 93 ka which may record changes in orbital precession and obliquity (Weedon, 1985/86). Carbonate production in pelagic mid-Cretaceous sediments, quantified by calcium carbonate and optical densitometry time series, reflects the orbital eccentricity and precessional cycles (Herbert and Fisher, 1986). Fourier analysis of long sections of the Late Triassic Lockatong and Passaic formation of the Newark Basin show periods in thickness corresponding roughly to the astronomical periodicities (Olsen, 1986). All these interesting results has encouraged research on the stability of the solar system in order to determine to which extent the changing Earth-Moon distance, for example, influenced the length of the main astronomical periods (Berger et al., 1989).

Besides the usual 100, 41, 23 and 19 ka-periods which characterize most of the late Pleistocene data, Ruddiman et al. (1986) succeeded in finding in the geological records one of the secondary astronomical periods that was already predicted by Berger (1977a), the 54 ka one. A similar period of 58 ka was found in a 400 ka record of the paleomagnetic field from Summer Lake in South-central Oregon (Negrini et al., 1988). Finally, combination tones have also been found in deep-sea cores with a high sedimentation rate (Pestiaux et al., 1988) and in the Vostok ice core over the last 140,000 years (Yiou et al., 1991).

A fairly coherent phase relationship was also reasonably well defined between insolation and ice volume in Kominz and Pisias (1979) where obliquity consistently lead the ^{18}O

record by about 10,000 years, whereas precession seemed to be in phase with the 23 ka geological signal. However, the recent results obtained by SPECMAP show that these leads and lags are more complicated. CLIMAP (1976) and more recently the SPECMAP (Imbrie et al., 1984) teams have indeed shown that the phase lags in the climate response to orbital forcing depend upon the nature of the climatic parameters themselves and upon their geographical location. For example in their data, the sea-surface temperature of the southern oceans seems to lead the response of the northern hemisphere ice sheets by roughly 3,000 years. The results of the SPECMAP Atlantic study reveal the lead of southern hemisphere responses ahead of the northern hemisphere and highest sensitivity of the high-latitude North Atlantic in all astronomical bands (Imbrie et al., 1989). Spectral analysis of a number of Atlantic time series illustrates quite well this spatial dependence of the frequency response of SST records, most of them showing distinct frequencies in the primary Milankovitch bands (Imbrie et al., 1989). In the obliquity band, there is relatively little response in low latitudes, except in a few records near the equator. In the precession band, there is a suggestion of a phase shift accross the equator; South Atlantic temperature changes lead oxygen isotopes (ice volume) and North Atlantic responses are either in phase or lag ice volume. The southern hemisphere phase leads also occurs in the 100-ka band. All (but one) SST phases at 100-ka are within 12,000 years of ice volume and eccentricity maxima.

This complexity is not too surprising as these spectra depend upon the way the climate system reacts to the insolation forcing and upon which type of insolation it is sensitive too. Contrary to the well-received Milankovitch idea that the high polar latitudes must record the obliquity signal (as shown in the Vostok core, for example, Jouzel et al., 1987) whereas low latitudes record only the precessional one, the latitudinal dependence of the insolation parameters is more complex. Clearly the mid-month high-latitude summer insolation displays a stronger signal in the precession band than in the obliquity one (Berger and Pestiaux, 1984).

2 The 100-ka Cycle

As already shown by Hays et al. (1976), the variance components centered near a 100 ka cycle, which dominates most upper Pleistocene climatic records, seem to be in phase with the eccentricity cycle (high eccentricity at low ice volume). Unfortunately, the in-

terpretation of the data is not always as clear. The 100 ka cycle, so dominant a feature of the late Pleistocene record, does not exhibit a constant amplitude over the past 2-3 million years. This periodicity seems to disappear before 10^6 years ago, at a time the ice sheets were much less developed over the Earth, reinforcing the idea that the growth of the major ice sheets may have played a role in the modulation of the 100 ka cycle. Spectral analysis of DSDP Hole 552A reveals indeed a dominant quasi-periodicity associated with obliquity-induced temperature variations in surface water and weaker peaks at the eccentricity and precession periods (Backman et al., 1986). More precisely, Shackleton et al. (1988) found a 100 ka-peak for the period 0 to 1 Ma BP, a 100 ka and a 41 ka-peaks for 0.5 to 1.2 Ma BP and mainly a 23 ka-one for 2.5 to 3.5 Ma BP, this section displaying however significantly less variance.

In any case, the amount of insolation perturbation at 100 ka is not enough to cause a direct climate change of ice-age magnitude. The exceptional strength of this cycle calls, therefore, for a stochastic (Hasselman, 1976; Kominz and Pisias, 1979) amplification of the insolation forcing, or for a non-linear amplification through the deep ocean circulation, the carbon dioxide, the ice sheet related feedbacks (Birchfield and Weertman, 1978; Pollard, 1984), the isostatic rebound of the lithosphere (Oerlemans, 1980) and/or the ocean-ice interactions. The 100 ka climatic cycle can indeed be explained both (i) from the eccentricity signal directly, provided an amplification mechanism can be found (as in the double potential theory of Nicolis 1980, 1982 and Benzi et al., 1982); and/or (ii) by a beat between the two main precessional components as shown by Wigley (1976) and Imbrie and Imbrie (1980) from non-linear climate theory. It is therefore very important to clearly explain the spectrum of the insolation and of the astro-climatic parameters which are used in climate model.

Recent ice sheet models show also that the 100 ka cycle can be simulated with (Ghil and Le Treut, 1981; Saltzman et al., 1984) or without (Lindzen, 1986) internal free oscillations related to resonances when astronomically forced. It is significantly reinforced when isostatic rebound (Hyde and Peltier, 1985) and iceberg calving are taken into account (Pollard, 1982).

Finally, it must be remembered that Milankovitch requested a high eccentricity for an ice age to occur - which is just the reverse of the correlation claimed by Hays et al. (1976). Considering only the caloric insolations developed to the first degree of eccen-

tricity, Milankovitch viewed indeed the effect of the eccentricity through the precessional parameter alone.

Facing all these problems related to the stability of the frequencies in space and time and to the origin of the 100 ka cycle, related to eccentricity or to precession, it seems worth to give some fundamentals about the formulas used to compute the insolations which force directly the climate system. This is expected to help identifying more easily the origin of the frequencies found in geological data.

3 Astronomical origin of the eccentricity cycles

The eccentricity, e, of the Earth's orbit around the Sun is a measure of its shape given by : $e^2 = \frac{a^2-b^2}{a^2}$, where a and b are the semi-major and semi-minor axes of the elliptical orbit. It is presently 0.016 and it has changed between 0 and 0.07 over the Quaternary with a highly variable periodicity which mean is roughly 100 ka (Berger, 1976). Its computation is obtained from solving the Lagrange equations of the motion of the planets around the Sun (Berger, 1977b). The trigonometrical series derived by Berger (1978), from the Bretagnon (1974)'s analytical solution of this system, is given by:

$$e = 0.0287 + \Sigma E_k \cos(\lambda_k t + \phi_k) \quad (1)$$

where the amplitudes, E_k, the mean rates, λ_k, and phases, ϕ_k are given in Table 3 of Berger (1978). The periods of the six terms corresponding to the largest amplitudes are recalled in Table 1. It is also interesting to give the corresponding periods of a more recent solution (Berger and Loutre, 1991) obtained from Laskar (1988)'s integration of the planetary system. The comparison between the two sets of values show the excellent accuracy with which these periods are presently determined.

Table 1: Period of the most important terms in the serie expansions of eccentricity, e, $e \sin \pi$, climatic precession, $e \sin \tilde{\omega}$ (Berger, 1978) and eccentricity again from Berger and Loutre (1991).

	Berger, 1978			Berger-Loutre, 1991
	eccentricity	$e \sin \pi$	$e \sin \tilde{\omega}$	eccentricity
1	412 885	308 043	23 716	404 178
2	94 945	176 420	22 428	94 782
3	123 297	72 576	18 976	123 818
4	99 590	75 259	19 155	98 715
5	131 248			130 615
6	2 035 441			2 379 077

This series (1) is originating from the expansion of

$$e = \sqrt{(e \sin \pi)^2 + (e \cos \pi)^2} \tag{2}$$

where the two terms $e \sin \pi$ and $e \cos \pi$ involve the longitude, π, of the perihelion measured from a fixed vernal equinox of reference (taken as the one of 1950 A.D.; for the explanation of the astronomical parameters see Figures 1 and 2). For the 1978 solution, the expansion of $e \sin \pi$ comes from the solution by Bretagnon (1974) and the amplitudes, mean rates and phases were calculated and given in Table 4 of Berger (1978). The four most important ones are recalled in Table 1. It can easily be shown that each period, PE, of the eccentricity is obtained as a combination of 2 periods, PP, of $e \sin \pi$, through:

$$\frac{1}{PE_k} = \frac{1}{PP_i} - \frac{1}{PP_j} \tag{3}$$

So the first six periods PE_k ($1 \leq k \leq 6$) of the eccentricity in (1) are respectively given by the combination of the periods PP numbers 2 and 1, 3 and 1, 3 and 2, 4 and 1, 4 and 2, 3 and 4.

But e can also be obtained through a relation similar to (2) involving the climatic precession, $e \sin \tilde{\omega}$, where $\tilde{\omega}$ is the longitude of the perihelion measured from the vernal equinox at a given date, t:

$$e = \sqrt{(e \sin \tilde{\omega})^2 + (e \cos \tilde{\omega})^2} \tag{4}$$

This climatic precession is a measure of the Earth-Sun distance at the summer solstice (see later formula 25). Its mean periodicity is 21 ka but its analytical expansion (or

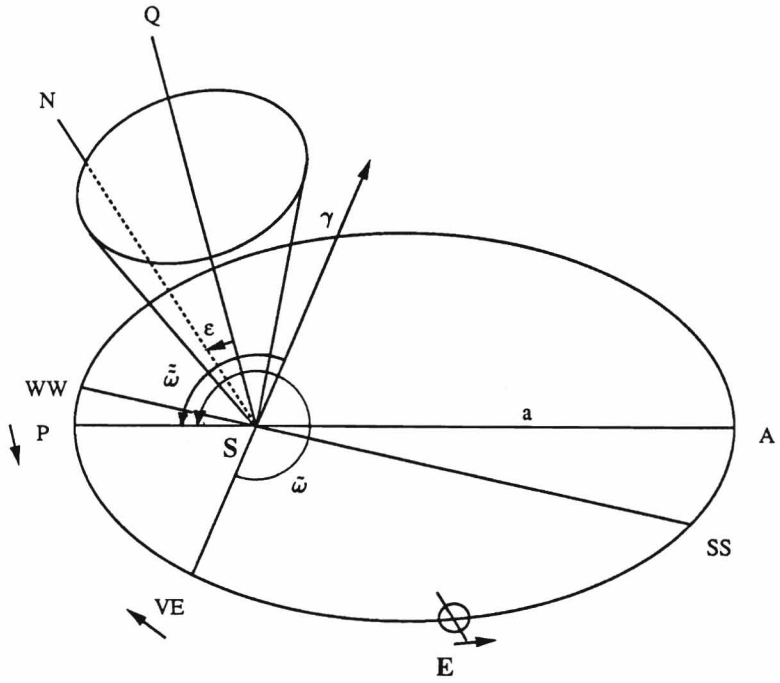

Figure 1: Elements of the Earth's orbit.

The orbit of the Earth, E, around the Sun, S, is represented by the ellipse PEA, P being the perihelion and A the aphelion. Its eccentricity e is given by $\frac{(a^2-b^2)^{1/2}}{a}$, a being the semimajor axis and b the semiminor axis. WW and SS are the winter and summer solstices, respectively; γ is the vernal point. WW, SS, and γ are approximately located where they are today. SQ is perpendicular to the ecliptic, and the obliquity ε is the inclination of the equator upon the ecliptic; i.e., ε is equal to the angle between the Earth's axis of rotation SN and SQ. Parameter $\tilde{\omega}$ is the longitude of the perihelion relative to the moving vernal equinox, and is equal to $\pi + \psi$. The annual general precession in longitude, ψ, describes the absolute motion of γ along the Earth's orbit relative to the fixed stars. The longitude of the perihelion, π, is measured from the reference vernal equinox of A.D. 1950 and describes the absolute motion of the perihelion relative to the fixed stars. $\tilde{\omega} = \tilde{\omega} - 180°$, is the longitude of the perihelion measured from γ; its numerical values are calculated in Berger (1978).

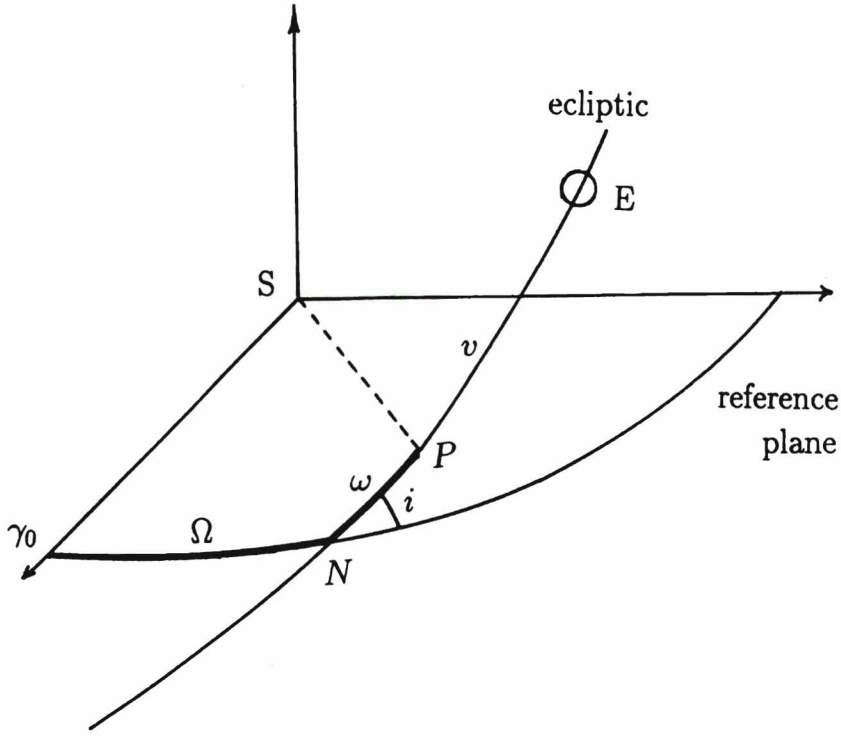

Figure 2: Position of the Earth (E) around the Sun (S).

In astronomy, it is usual to define an orbit and the position of the body describing that orbit by six quantities called the elements. Three of them define the orientation of the orbit with respect to a set of axes, two of them define the size and the shape of the orbit (a and e respectively), and the sixth (whith the time) defines the position of the body within the orbit at that time. In the case of a planet moving in an elliptic orbit about the Sun, it is convenient to take a set of rectangular axes in and perpendicular to the plane of reference, with the origin at the centre of the Sun. The x-axis may be taken towards the ascending node N, the y-axis being in the plane of reference and 90^o from x, while the z-axis is taken to be perpendicular to this reference plane so that the three axes form a right-handed coordinate system. γ_0 is the reference point from where the angle are measured. As the reference plane is usually chosen to be the ecliptic at a particular fixed date of reference (named epoch of reference in celestial mechanics; Woolard and Clemence, 1966), γ_0 is, in such a case, the vernal point at that fixed date (the vernal point is also referred to as the First Point of Aries indicating the position of the Sun when it crosses the celestial equator from the austral to the boreal hemisphere). P is the perihelion; Ω the longitude of the ascending node; ω, the argument of the perihelion; $\pi = \Omega + \omega$ the longitude of the perihelion; i the inclination; v the true anomaly; $\lambda = \pi + v$ the longitude of the Earth in its orbit.

spectrum in the frequency domain) given by:

$$e \sin\tilde{\omega} = \Sigma P_k \sin(\alpha_k t + \zeta_k) \quad (5)$$

shows clearly two main periods averaging close to 23 ka and 19 ka (see Table 1 of this paper or Table 2 of Berger, 1978).

The calculation of $\tilde{\omega}$ is more complex than of π as it requests to consider also the motion of the Earth's axis of rotation. This involves the astronomical precession (the so-called general precession in longitude, ψ) and the obliquity, ϵ. The astronomical precession is describing the absolute motion of the vernal equinox in time and its period to circle around the Earth's orbit is roughly 26,000 years. The combination of the absolute motion (counterclockwise) of the perihelion given by π and of the absolute motion (clockwise) of the vernal equinox given by ψ provides the relative motion of the perihelion against the vernal equinox, $\tilde{\omega} = \pi + \psi$. On the other hand, the obliquity is the tilt of the equator on the Earth's orbit. Its present value is $23°27'$. It has varied over the Quaternary from $22°30'$ to $25°$ approximately, with a mean period of 41 ka.

Although the origin of the period of each term in (5) is difficult to trace back (Berger and Loutre, 1990), it is also possible to use a relation similar to (3) where the PP's are now those related to $e \sin\tilde{\omega}$ to find the origin of the PE_k. These PE_k ($1 \leq k \leq 6$) related to the α_k of (5) are obtained respectively from the combination of the following periods of $e \sin\tilde{\omega}$: 2 and 1, 3 and 1, 3 and 2, 4 and 1, 4 and 2, and 3 and 4. This technique was used by Berger (1973), noted partly from numerical investigation by Stothers (1987) and demonstrated fully in a comprehensive paper by Berger and Loutre (1990).

So very clearly, the eccentricity periods in celestial mechanics can be expressed as combinations of the precessional periods themselves.

4 Energy received by the whole Earth over a full year

If S_a is the solar energy received by unit of time on a surface of unit area perpendicular to the Sun rays and situated at the distance a from the Sun (a is equal to the semi-major axis of the Earth's orbit), the total energy W received by the Earth at the distance r

from the Sun is equal to

$$W_E = S_a \left(\frac{a}{r}\right)^2 \pi R^2 \tag{6}$$

R being the Earth's radius.

Over a complete year of length T, the energy, W_E^T, received by the whole Earth, will be

$$W_E^T = \int_0^T W_E dt = S_a \, \pi R^2 \int_0^T \left(\frac{a}{r}\right)^2 dt \tag{7}$$

As we see from (7), we must compute the mean value of $(\frac{1}{r})^2$ over the whole year:

$$< \frac{1}{r^2} > = \frac{1}{T} \int_0^T \frac{1}{r^2} \, dt$$

This can easily be done by using the second law of Kepler

$$\frac{r^2}{2} \frac{dv}{dt} = \frac{\pi a^2}{T} \sqrt{1 - e^2} \tag{8}$$

where v is the true anomaly of the Earth on its elliptical orbit (Figure 2).

Replacing (8) in (7) leads to:

$$W_E^T = S_a \, \pi R^2 \int_0^{2\pi} \frac{T}{2\pi} \frac{1}{\sqrt{1 - e^2}} \, dv$$

Assuming that e is constant over one year (we recall that e varies between 0 and 0.07 in 100,000 years at the maximum), we obtain:

$$W_E^T = \frac{S_a}{\sqrt{1 - e^2}} \pi R^2 T \tag{9}$$

As a is secularly invariable (at least to an excellent accuracy as demonstrated in celestial mechanics), T is also invariable as seen from the third law of Kepler:

$$\frac{4\pi^2}{T^2} a^3 = const.$$

Therefore, W_E^T is only a function of the energy output from the Sun through S_a and of the eccentricity of the Earth's orbit through $(1 - e^2)^{-\frac{1}{2}}$.

The integration of (6) shows that the mean value of $(\frac{a}{r})^2$ over one year is equal to $(1 - e^2)^{-\frac{1}{2}}$. If we denote r_m the constant value of r which satisfies the following relation:

$$< \frac{a^2}{r^2} > \equiv \frac{1}{T} \int_0^T \left(\frac{a}{r}\right)^2 dt = \frac{1}{\sqrt{1 - e^2}} \tag{10}$$

we obtain

$$r_m^2 = a^2 \sqrt{1-e^2} \tag{11}$$

r_m can also be considered as the radius of a circle which has the same area as the elliptical orbit of the Earth around the Sun. r_m is thus the mean value of r, energetically speaking, because the total energy received by the Earth over a whole year (9) is the same as that received by a fictitious Earth revolving around the Sun at a constant distant r_m (see Appendix 1 for the arithmetic mean of r). If we denote S_0 the energy received by unit of time on a unit area perpendicular to the Sun rays and situated at this mean distance r_m from the Sun, S_0 is the so-called solar constant and we have:

$$4\pi a^2 \, S_a = 4\pi r_m^2 \, S_0$$

which means:

$$S_a = S_0 \, (\frac{r_m}{a})^2$$

Through (11) we obtain $S_a = S_0 \sqrt{1-e^2}$

or

$$S_0 = \frac{S_a}{\sqrt{1-e^2}} \tag{12}$$

S_0 is, actually, not a true constant and it would be more appropriate to call it solar parameter, for example. It depends indeed (see (12)) upon the solar output, which is determined from observations and studied from theoretical investigations of the solar activity and luminosity, and upon the mean distance from the Earth to the Sun.

The energy received by the whole Earth over one year becomes

$$W_E^T = S_0 \, \pi R^2 T \tag{13}$$

(13) is evidently equivalent to (9) except that (13) is an implicit function (not explicit as in (9)) of e through (12).

If we denote by $\overline{W}_E$ the energy received per unit of the Earth's surface and per unit of time calculated for a full year, (9) and (13) give:

$$\overline{W}_E = \frac{S_0}{4} = \frac{S_a}{4\sqrt{1-e^2}} \tag{14}$$

which is presently estimated to be roughly 340 Wm^{-2} (Lean, 1991).

Although the absolute effect of the factor $(1-e^2)^{-1/2}$ is relatively small (a few per mil at the most), this term increases the annual global insolation at high eccentricity

and decreases it at low eccentricity. As compared to present-day value ($e = 0.016$), W_E increases by 0.27 % (3.7 Wm^{-2} over 1360 Wm^{-2}) for $e = 0.075$ and decreases by 0.01 % (0.17 Wm^{-2} over 1360 Wm^{-2}) for $e = 0$. This behaviour is coherent with the Hays et al. (1976) and others' result showing, over most of the upper Quaternary, low ice volume at high eccentricity. It is obvious that if we simplify (9) or (14) by omitting the term in e^2, this kind of behaviour cannot be seen: in such a case, r_m is approximated by a, as it was unfortunately too frequently assumed.

Let us finally note that the expansion of $(1-e^2)^{-\frac{1}{2}}$ to the second degree in eccentricity leads to:

$$\overline{W}_E = \frac{S_a}{4}\left(1 + \frac{e^2}{2}\right) \tag{15}$$

and therefore the variation around a reference value denoted by the subscript 0 can be approximated by:

$$\Delta\overline{W}_E = \overline{W}_E - \overline{W}_{E,o} = \frac{S_a}{8}\Delta(e^2) = \frac{S_a}{4}\,\overline{e}\,\Delta e \tag{16}$$

where $\overline{e} = \frac{e+e_o}{2}$ and $\Delta e = e - e_o$

5 Insolation of the Earth at a given instant of time and latitude

At a given instant during the course of the year, corresponding to a declination δ of the Sun and to a distance r, the insolation, W, received on a horizontal surface located at a latitude ϕ is given by (Figure 3 and Berger et al. (1993b) for more details):

$$W = S_a \left(\frac{a}{r}\right)^2 \cos z \tag{17}$$

where z is the zenith distance of the Sun given by:

$$\cos z = \sin\phi \sin\delta + \cos\phi \cos\delta \cos H \tag{18}$$

- δ is related to the true longitude of the Sun, λ, by:

$$\sin\delta = \sin\lambda \sin\epsilon \tag{19}$$

Over one year, δ varies between two extreme values, $-\epsilon$ and $+\epsilon$, whereas λ varies from 0 to 360°. But because of (19) and the long-term variations of ϵ, the insolation

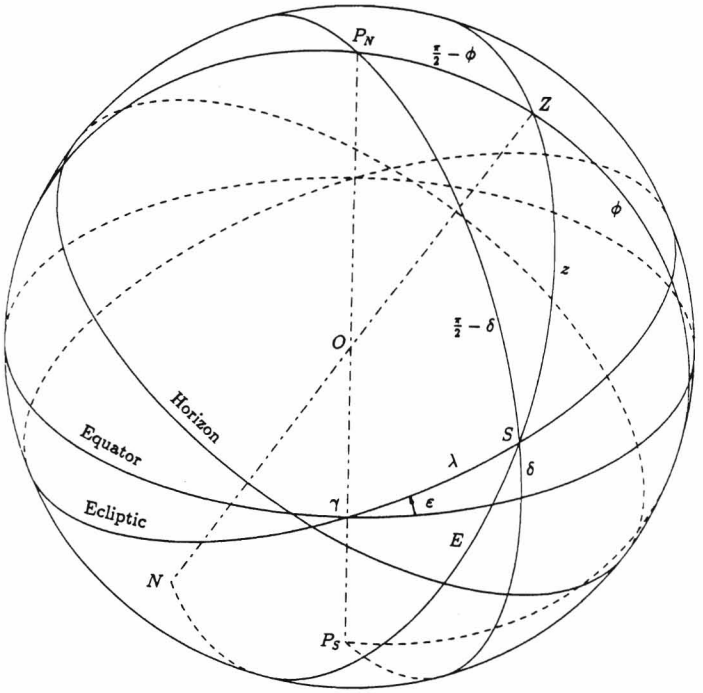

Figure 3: Position of a point (S) on the celestial sphere (Woolard and Clemence, 1966). The astronomical horizon is the great circle in which the celestial sphere is intersected by the plane that passes through the observer (O) and is perpendicular to the direction of the local gravity. The zenith (Z) is the point vertically upward or overhead. The nadir (N) is the point diametrically opposite the zenith. The vertical circles are the great circles through the zenith and nadir, and therefore necessarily perpendicular to the horizon. The two diametrically opposite points on the celestial sphere, which mark the ends of the axis of the apparent diurnal rotation of the sphere are called celestial poles (P_N, P_S). The great circle of the celestial sphere midway between the poles is the equator. Great circles through the poles are called secondary circles. The zenith distance (z) of any point on the celestial sphere is the angular distance from the zenith measured along the vertical circle through the given point. It varies from 0 to 180°. It is complementary to the altitude E. The position of any point on the celestial sphere can also be measured by the angle between the meridian (great circle through the poles, the zenith and the nadir) and the secondary through the point. This angle is called hour angle (H). The declination (δ) is the angular distance of the point from the equator measured on the secondary. The latitude of the observer, ϕ, is the angular distance from the equator to the zenith measured on the meridian. The longitude of the point (S) on its orbit is the angular distance from the vernal point on the ecliptic. The obliquity, ϵ, is defined as in Figure 1.

at a given δ fixed through time does not correspond always to the same position of the Earth about the Sun given by λ.

- H is the hour angle of the Sun which defines the time of the day. In time units, it is related to the legal time, TL, through

$$H = TL + FH - WT - 12 - LG + ET \tag{20}$$

where FH is the number of the time-zone (0 for Greenwich and positive to the west), WT allows to define the summer time and the winter time (e.g., in Europe $WT = 1$ for summer and 0 for winter), LG is the geographical longitude expressed in time units and measured positively to the west and ET the equation of time which is independent of the latitude and is only a function of the day (presently, its minimum value is -14 minutes on 11 February and its maximum is reached on 3 November with +16 minutes).

- r, the Earth-Sun distance, is given by the ellipse equation:

$$r = \frac{a(1-e^2)}{1+e\,\cos v} \tag{21}$$

- v being the true anomaly related to the true longitude, λ, of the Earth by

$$\lambda = v + \tilde{\omega}\,. \tag{22}$$

As in this formula, $\tilde{\omega}$ is measured from the vernal equinox, 180° has to be added to the numerical value calculated by Berger (1978). This is related to the fact that, in practice, the numerical calculations are done using as a reference the direction in which the Sun is seen from the Earth at the beginning of the spring, the so-called vernal point γ defining therefore the angle $\tilde{\tilde{\omega}}$ on Figure 1 with clearly $\tilde{\omega} = \tilde{\tilde{\omega}} + 180°$.

The following relationships obtained from (21):

$$r_{\text{perihelion } (v=0°)} = a(1-e) \tag{23}$$

$$r_{\text{aphelion } (v=180°)} = a(1+e) \tag{24}$$

show that the normalized distance (r/a) from the Earth to the Sun varies in the course of the year by $2e$, which means that the corresponding energy received by the Earth varies as $4e$, reaching a maximum of 30 % roughly (for $e = 0.075$) over the Quaternary.

Moreover

$$r_{\text{summer solstice } (\lambda=90^\circ)} = \frac{a(1-e^2)}{1+e\,\sin\tilde{\omega}} \sim a(1 - e\,\sin\tilde{\omega}) \tag{25}$$

$$r_{\text{winter solstice } (\lambda=270^\circ)} = \frac{a(1-e^2)}{1-e\,\sin\tilde{\omega}} \sim a(1 + e\,\sin\tilde{\omega}) \tag{26}$$

$$r_{\text{spring equinox } (\lambda=0^\circ)} = \frac{a(1-e^2)}{1+e\,\cos\tilde{\omega}} \sim a(1 - e\,\cos\tilde{\omega}) \tag{27}$$

$$r_{\text{fall equinox } (\lambda=180^\circ)} = \frac{a(1-e^2)}{1-e\,\cos\tilde{\omega}} \sim a(1 + e\,\cos\tilde{\omega}) \tag{28}$$

For $e = 0.016$ and $\tilde{\omega} = 282^o$ which are present day conditions, we have therefore $\frac{r}{a}$ equals to 0.984 at the perihelion, 1.016 at the aphelion, 1.016 at summer solstice, 0.984 at winter solstice, 0.996 at the vernal (spring) equinox and 1.003 at the autumnal (fall) equinox. The seasonal contrast of $\frac{r}{a}$ measured by the difference between the winter and summer solstices is therefore equal to $2\ e\ \sin\tilde{\omega}$, which represents today a value slightly over 3 %, but can amount up to 15 %. The maximum and minimum contrasts are reached at high excentricity and for the summer solstice occuring respectively at perihelion and at aphelion.

With (18) and (21), (17) becomes:

$$W = S_a \frac{(1+e\,\cos v)^2}{(1-e^2)^2} (\sin\phi\,\sin\delta + \cos\phi\,\cos\delta\,\cos H) \tag{29}$$

Over a given year, ϵ, e and $\tilde{\omega}$ are assumed to be constant; over a given day, λ and δ are assumed to be constant and H varies from 0 at solar noon to 360° (or from 0 to 24h).

The long-term variation for a given latitude, day and hour thus clearly depends upon e, $\tilde{\omega}$ which appear in (29) through (22) and ϵ which is implicitely contained in δ according to (19). Moreover, the behaviour of each factor in (29) is governed by a different orbital parameter: ϵ drives the long term variation of $\cos z$, $\tilde{\omega}$ the long term variation of $(1 + e\,\cos(\lambda - \tilde{\omega}))^2$ and e the long term variation of $(1 - e^2)^2$. This last factor is particularly interesting and it must be recognized that the daily insolation is depending upon $(1-e^2)^{-2}$ and not upon $(1 - e^2)^{-1/2}$ which drives the total energy received by the Earth over one year (see (14)).

However, W depends also upon e through $(1 + e \cos v)^2$. In the formula (29), the distance factor $\rho^{-2} = (\frac{a}{r})^2$ can indeed be written:

$$\frac{1 + 2e\cos v + e^2\cos^2 v}{(1-e^2)^2} = (1 + 2e\cos v + \frac{e^2}{2}\cos 2v + \frac{e^2}{2})(1-e^2)^{-2}$$

and $(1-e^2)^{-2}$ can be developed to an excellent accuracy:

$$(1-e^2)^{-2} \sim 1 + 2e^2 + \text{terms of order 4 and over}$$

which leads finally to:

$$\left(\frac{1 + e\cos v}{1-e^2}\right)^2 \sim 1 + 2e\cos v + \frac{e^2}{2}\cos 2v + \frac{5e^2}{2} + 4e^3\cos v \qquad (30)$$

neglecting all terms of power 4 and over in eccentricity (this corresponds to an accuracy of 10^{-5} at the minimum).

Being given the definition of $v = \lambda - \tilde{\omega}$ and for a given value of λ, the spectrum of ρ^{-2} must therefore be dominated by the climatic precession ($e\sin\tilde{\omega}$ or $e\cos\tilde{\omega}$) displaying mainly 23 and 19 ka periods (Berger, 1977a). Moreover, this spectrum must also show, with a much less power, half precession periods (11.5 and 9.5 kr) because we have in (30) a term in $e\cos 2(\lambda - \tilde{\omega})$ weighted by $\frac{e}{2}$. Small spectral power at the eccentricity periods (400 and 100 ka) are also expected through the term $\frac{5e^2}{2}$. Finally, combination tones are awaited from the third term on. These analytical results are confirmed by spectral analyses which shows clearly, for spring equinox ($v = -\tilde{\omega}$) and summer solstice ($v = 90^o - \tilde{\omega}$), strong precessional peaks, weak peaks at the eccentricity and half precession periods and some other combination tones (Figures 4 and 5).

Finally, this formula (29) has the advantage to show that, for a given λ, the precession and obliquity signals originate from two distinct factors with a clear physical meaning: the precession signal originates from the distance factor (ρ^{-2}) and the obliquity signal comes from the inclination factor ($\cos z$). Therefore, for any fixed distance from the Earth to the Sun, there is only an obliquity signal in the insolation through geological times and for a fixed zenith distance (or altitude) there can only be a precessional signal. Consequently, for a given hour of a particular day, defined by a given value of λ, W is mainly a function of both precession and obliquity, the spectral amplitude at these frequencies depending upon the latitude and upon the time of the year ; it is also a function of eccentricity but with much less power.

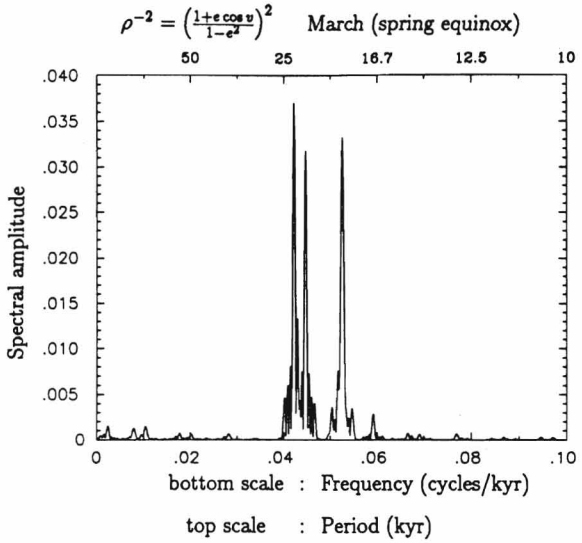

Figure 4: Spectral amplitude in the Thomson multi-taper harmonic analysis, at spring equinox (March), of $\rho^{-2} = \left(\frac{1+e\cos v}{1-e^2}\right)^2$.

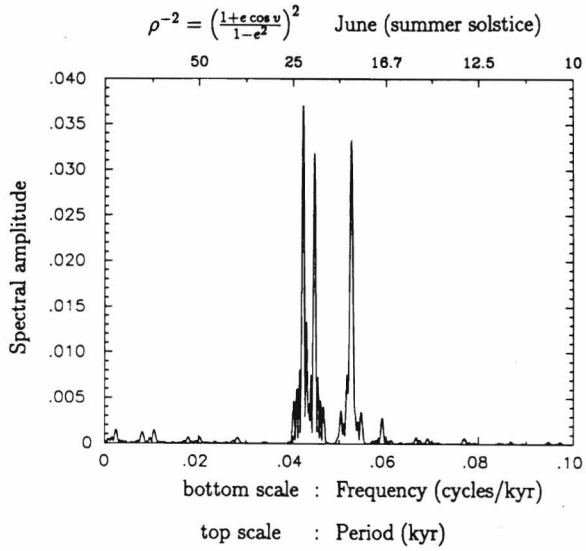

Figure 5: Spectral amplitude in the Thomson multi-taper harmonic analysis,at summer solstice (June), of $\rho^{-2} = \left(\frac{1+e\cos v}{1-e^2}\right)^2$.

However, if we would like to compare, for different geological times, the irradiances received on an horizontal surface for the same inclination of the sunrays, we must consider the insolation at fixed z (or altitude h) which clearly does not correspond to a fixed H; H being related to z through (18), we have indeed:

$$\cos H = \frac{\cos z - \sin\phi \sin\delta}{\cos\phi \cos\delta} \tag{31}$$

For any λ, except $\lambda = 0$ and $180°$, the variation through time of the hour angle corresponding to a fixed z shows only a strong obliquity quasi-periodicity.

For the sake of comparing insolations in the same physical and astronomical contexts, it is the insolations at a fixed value z which must be intercompared from one geological time to another. It means, that the spectrum of (17) is strictly the one of ρ^{-2}. Again, as (30) shows for a fixed λ, there is no power of obliquity in such calculation.

In such conditions, the instantaneous insolation given by (17), i.e. $W = \frac{S_a}{\rho^2} \cos z$, can be computed for each value of z situated between $90°$ and z_{min} for each latitude for which there is a sunrise and a sunset ($z = 90°$). z_{min}, which corresponds to $H = 0$, is given by $\cos z_{min} = \cos(\phi - \delta) = \sin\phi \sin\lambda \sin\epsilon + \cos\phi\sqrt{1 - \sin^2\lambda \sin^2\epsilon}$ as it can be deduced directly from (18) and (19). For the long day during which the Sun does not set, the maximum value of z is reached at midnight for $H = 180°$ (or 12h), which means:

$$\cos z_{max} = -\cos(\phi + \delta) = \sin\phi \sin\lambda \sin\epsilon - \cos\phi \sqrt{1 - \sin^2\lambda \sin^2\epsilon}$$

However if the diurnal cycle of insolation has to be calculated, as it is the case in climate model, irradiance for different values of H will be used. As we just pointed out, for a fixed ϕ and λ, one given value of H does not obviously correspond to the same z all the time, the relation depending upon the obliquity. According to (18) and (19) for the fixed values of H, the corresponding $\cos z$ can indeed be calculated from:

$$\cos z = \sin\phi \sin\lambda \sin\epsilon + \cos\phi\sqrt{1 - \sin^2\lambda \sin^2\epsilon}\cos H \tag{32}$$

6 Perihelion and the astronomical seasons

Among all possible values of v over one year ($0 \leq v \leq 360^o$), the following ones illustrate the total effect of the eccentricity alone:

$$\text{at the perihelion } (v = 0^o): \quad W^P = S_a \frac{1}{(1-e)^2} \cos z \tag{33}$$

$$\text{at the aphelion } (v = 180^o): \quad W^A = S_a \frac{1}{(1+e)^2} \cos z \tag{34}$$

$$\text{at orthogonal distance } (v = 90^o \text{ or } 270^o): \quad W = S_a \frac{1}{(1-e^2)^2} \cos z \tag{35}$$

Taking 0.075 as a maximum value of e, the factors containing e vary with a maximum amplitude of respectively 17, 13 and 1 %. Although it is interesting to see that these insolations are only functions of obliquity and eccentricity and not of precession, one must recognize that the perihelion drifts continuously through all the seasons according to the long term variation of its longitude.

By fixing arbitrarily the spring equinox at 21 March, the Earth is indeed at the perihelion, for example at 14 September, 1 February, 22 April, 13 July, 3 September and 3 January for respectively 122 ka, 20 ka BP, 15 ka BP, 10 ka BP, 7 ka BP and now. This is also reflected by the long term variation of the length of the astronomical seasons which is only a function of the climatic precession (Berger and Pestiaux, 1984; see also Annex 2). If we consider the astronomical spring, summer, fall and winter, their length varies over the last 10^6 years between 82.5 and 100 mean solar days. Some examples are given for the same dates as above in Table 2.

These examples illustrate how complex the relationship between the insolations and the orbital parameters is. It also underlines the importance that the eccentricity can have individually; terms containing e alone cannot be ignored, especially since they reinforce the impact on climate in the explanation of the strength of 100 ka cycle. On the other hand, the insolations are involved, in intricated ways, in a number of non-linear processes in the climate system. These can distord the input signal both in amplitude and frequency. The physical mechanisms through which the climate system would response to such a given forcing are thus very difficult to conceive and cannot be deduced by only comparing the spectra of the input (insolation) and of the output (the geological records) signals. Physical models of the climate system will provide a complementary and neces-

sary information to analyse the complex way through which the system is responding to the astronomical forcing (Gallée et al., 1992; Berger et al., 1993a).

Table 2: Length of the astronomical spring, summer, fall and winter in mean solar days for 6 selected times of the past

date ka	Spring $0 \leq \lambda < 90°$	Summer $90° \leq \lambda < 180°$	Fall $180° \leq \lambda < 270°$	Winter $270° \leq \lambda < 360°$
122	95.7	86.2	87.0	96.4
20	91.5	94.5	91.1	88.2
15	88.2	92.0	94.5	90.6
10	90.2	88.3	92.4	94.3
7	92.8	88.6	89.8	94.0
0	92.8	93.6	89.8	89.0

7 Daily cycle of insolation

Sunset or sunrise correspond to z=90°, which means from (18):

$$\sin\phi \sin\delta + \cos\phi \cos\delta \cos H = 0$$

This gives the absolute value of the hour angle, H_o, at sunrise ($H = -H_o$) and sunset($H = H_o$):

$$\cos H_o = - \tan\phi \tan\delta \tag{36}$$

H_o does exist only for: $-1 \leq \tan\phi \tan\delta \leq +1$ which means that the latitudes for which there is a daily sunset and sunrise are given by

$$-(90° - |\delta|) \leq \phi \leq (90° - |\delta|) \tag{37}$$

Therefore, the latitudes where there is no sunset (H_o = 12h) are defined by:

$$|\phi| > 90° - |\delta| \text{ with} \begin{cases} \phi > 0 & \text{if } \delta > 0 \\ \phi < 0 & \text{if } \delta < 0 \end{cases} \tag{38}$$

and the latitudes where there is no sunrise ($H_o = 0$)

$$|\phi| > 90° - |\delta| \text{ with} \begin{cases} \phi > 0 & \text{if } \delta < 0 \\ \phi < 0 & \text{if } \delta > 0 \end{cases} \tag{39}$$

For $\delta = 0$, the length of the day is everywhere 12 hours, except at the poles which are singular points where H_o is set to 0. For $\phi = 0$ the length of the day is always equal to 12 hours according to (36). The solar zenith distance, z, (or altitude above horizon, $h = 90^o - z$) varies during the course of a day between extreme values which correspond to H equal to 0 (at solar noon) and 180^o (at midnight), if we account for the values of z and h corresponding also to the Sun below the horizon (in such a case $0 \leq z \leq 180^o$ and $-90^o \leq h \leq 90^o$).

For any value of ϕ and δ, we have

$$\text{for } H = 0: \quad z_{min} = |\phi - \delta| \qquad h_{max} = 90^o - |\phi - \delta| \tag{40}$$

$$\text{for } H = 180^o: \quad z_{max} = 180^o - |\phi + \delta| \quad h_{min} = -90^o + |\phi + \delta| \tag{41}$$

where z_{max} and h_{min} are therefore giving numerical values also for the Sun below the horizon. (We must point out that for the days where there is a sunset and sunrise, the values of z and h traditionally given are those for which $-H_0 \leq H \leq H_0$; in such cases, $z_{max} = 90^o$ and $h_{min} = 0$).

Allowing a complete cycle for $0 \leq H \leq 360^o$, the following relationships might be useful:

$$\begin{aligned}
h(\phi, \delta, H) &= h(-\phi, -\delta, H) \\
h_{\max}(\delta, \phi) &= h_{\max}(-\delta, -\phi) \\
h_{\min}(\delta, \phi) &= h_{\min}(-\delta, -\phi) \\
h_{\max}(\delta, \phi) &= -h_{\min}(\delta, -\phi) \\
h_{\max}(\delta, \phi) &= -h_{\min}(-\delta, \phi)
\end{aligned}$$

Figure 6 illustrates how h is varying all over the day ($-180^o \leq H \leq 180^o$) for any positive value of δ. For $\delta < 0$, a similar figure can be drawn easily from:

$$h(\phi, \delta, H) = h(-\phi, -\delta, H)$$

We want to stress that the derivative of this function $h(\phi, \delta, H)$ with respect to H at a given time in the year (δ) does not exist in two cases: when $\phi = \delta$ at $H = 0$ and when $\phi = -\delta$ at $H = 180^o$.

Figure 7 gives the variation of $h_{\max}$ and $h_{\min}$ at a particular date given for a positive value of δ (here $\delta = 23^o27$, the present-day value of ϵ). For a day with $\delta < 0$, we have

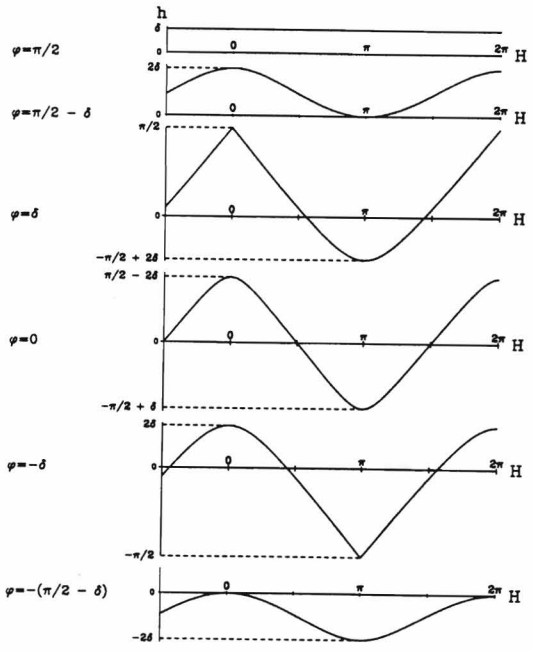

Figure 6: Variation of the altitude (h) all over the day ($-180^o \leq H \leq 180^o$) for any positive value of δ. For δ negative the same figure can be drawn easily from: $h(\phi, \delta, H) = h(-\phi, -\delta, H)$.

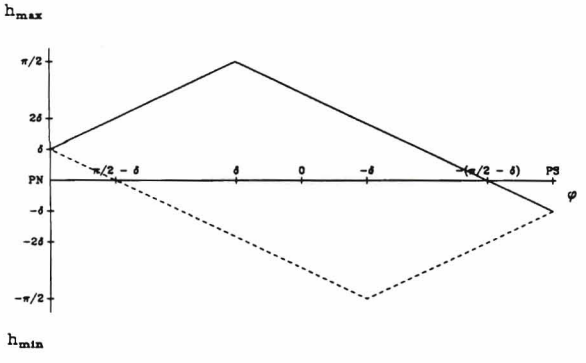

Figure 7: Variation of h_{max} and h_{min} at a particular date given for a positive value of δ. For $\delta < 0$, we have the same drawing with $h_{max}(-\delta, -\phi) = -h_{min}(\delta, -\phi)$ and $h_{min}(-\delta, -\phi) = -h_{max}(\delta, -\phi)$.

the same drawing but with

$$h_{\max}(-\delta,\phi) = -h_{\min}(\delta,\phi)$$
$$h_{\min}(-\delta,\phi) = -h_{\max}(\delta,\phi)$$

However, in the calculation of the energy received from the Sun, it is obvious that the maximum value allowed for z is 90^o and the minimum value allowed for h is 0, both occuring for $H = \mid H_0 \mid$, when the Sun sets or rises. The advantage of (41) is nevertheless to allow an easy calculation of the minimum value of the altitude of the Sun above the horizon during the course of the long day in polar latitudes.

8 Insolation at solar noon

At solar noon (i.e. for $H = 0$), W is given by:

$$W_{Noon} = S_a \frac{(1 + e\ \cos v)^2}{(1 - e^2)^2} \cos(\phi - \delta) \tag{42}$$

The obliquity signal is only present in the $\cos(\phi - \delta)$ factor if we choose a day of the year defined by a given value of λ:

$$\cos(\phi - \delta) = \sin\phi\ \sin\epsilon\ \sin\lambda + \cos\phi \sqrt{1 - \sin^2\epsilon\ \sin^2\lambda}$$

If the chosen day is defined by a fixed value of δ, there is no contribution of $\cos(\phi-\delta)$ to the spectrum of W_{Noon} and according to (30), $\frac{(1+e\cos v)^2}{(1-e^2)^2}$ will provide a spectral power at the frequencies of eccentricity and precession and at linear combinations between frequencies of eccentricity, precession and obliquity (due to λ which varies at the obliquity frequencies for a given δ according to (19)).

Moreover, as ϵ is only varying within a small range, W_{Noon} is dominated by precession everywhere, except maybe at high latitudes for small eccentricity values where obliquity contributes also significantly to the variation of W_{Noon} (Figure 8).

1. This is trivial for $\phi = \delta$, i.e. for those latitudes and days where the Sun reaches the zenith (z=0) at noon (for such a day δ, the maximum energy is reached over the Earth for $\phi = \delta$). For z=0, (42) becomes:

$$W_{Noon} = S_a \frac{(1 + e\ \cos v)^2}{(1 - e^2)^2} \tag{43}$$

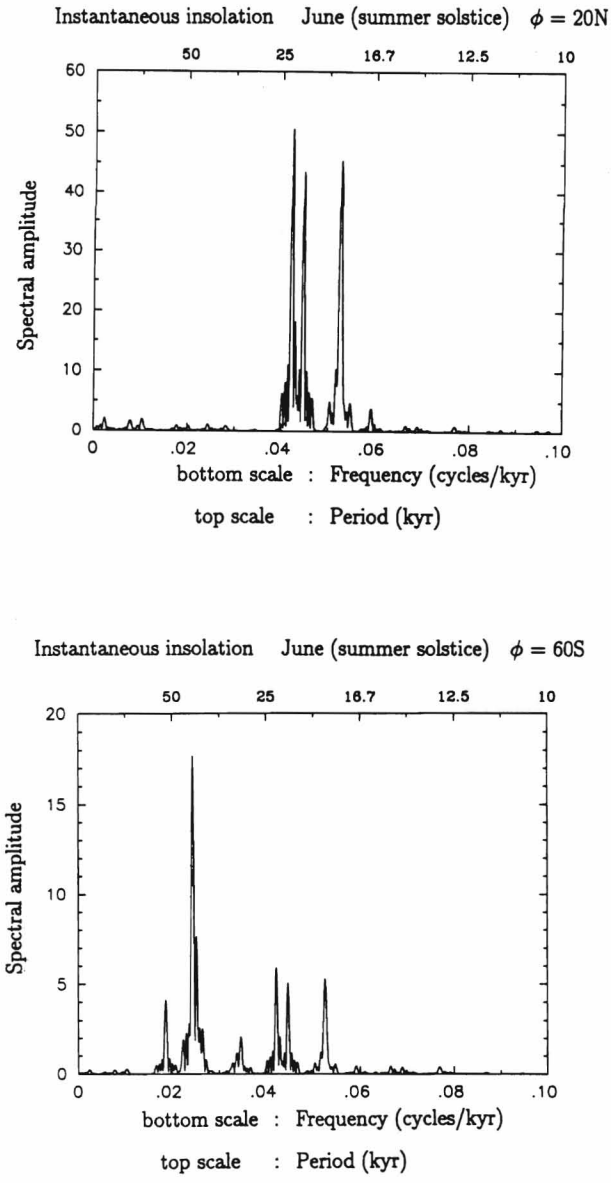

Figure 8: Spectral amplitude in the Thomson multi-taper harmonic analysis for summer solstice (June) of the instantaneous insolation at noon at 20N (top panel) and at 60S (bottom panel).

and there is obviously no obliquity signal in W_{Noon} for all those latitudes situated between the tropics and defined by $\mid \phi \mid \leq \epsilon_{min}$, provided the time of the year is selected according to $\delta = \phi$. The behaviour of (43) is dominated by precession, slightly modulated by the eccentricity. However, as δ is a function of the true longitude of the Sun through the obliquity (see 19), the position of the Earth relatively to the Sun (for a given value of δ) is not always the same through geological times, except for the equinoxes where $\lambda = 0$ and 180^o correspond always to $\delta = 0$. For the solstices $\lambda = 90^o$ and 270^o, $\delta = \epsilon$ and $-\epsilon$ respectively and varies at the astronomical time scale. In other words, the latitudes for which the Sun is at the zenith at noon at the solstices (the latitudes of the tropics defined by $\mid \phi \mid = \epsilon$) changes therefore in time with ϵ.

2. For the other latitudes, Table 3 gives the relative contribution of $\cos(\phi - \delta)$ to W_{Noon}, both at the equinoxes and northern hemisphere summer solstice, for two extreme values of ϵ.

   For $\delta = 0$, the change related to $\cos(\phi - \delta)$ is evidently strictly equal to zero for a given fixed ϕ; it is not for the polar and tropical circles which do not correspond to a fixed ϕ but varies in time with ϵ. ($\cos(\phi - \delta)$ is respectively equal to $\sin\epsilon$ and $\cos\epsilon$). The present-day latitudes of the polar circles are $66^o33'$ N and S. Over the Quaternary, as we have roughly $22^o \leq \epsilon \leq 24^o\ 30'$, the southernmost position of the arctic circle is $65^o\ 30'$ and its northernmost position is 68^o. At the birth of Christ, 2000 years ago, the latitude of the arctic circle was $66^o\ 18'$; within 2000 years it will be $66^o\ 49'$, which means that its motion towards north is presently around 14.4 m per year.

   At the summer solstice for which $\delta = \epsilon$ is varying in time, the absolute change of W_{Noon} due to obliquity factor is 7 % at the maximum (0.64 to 0.71); this maximum change is reached for the tropical circle of the winter hemisphere where $\cos(\phi - \delta) = \cos 2\epsilon$. The relative change can however reach more than 10 %. This is the case for the northern pole for which $\cos(\phi - \delta) = \sin\epsilon$ and for the high southern polar latitudes, north of the antarctic polar circle. The impact of the variation of $\cos(\phi - \epsilon)$ is indeed maximum for the maximal value of $\sin(\phi - \epsilon)$, it means for $\phi = -90^o + \epsilon$, the latitude of the antarctic circle. Consequently a small variation of the altitude of the Sun above the horizon, due to the variation of the obliquity, has much more influence in the frequency domain on $\cos(\phi - \epsilon)$ and therefore on insolation, when

Table 3: Contribution of $\cos(\phi - \delta)$ to the insolation at solar noon for some latitudes, at the spring equinoxe ($\delta = 0$) and summer solstice ($\delta = \epsilon$), for two extreme values of ϵ. Δ gives the relative change in % of this contribution when going from ϵ_{min} to ϵ_{max}.

	ϕ	$\delta = 0$		Δ	$\delta = \epsilon$		Δ
		$\epsilon = 22°30'$	$\epsilon = 25°$	(%)	$22°30'$	$25°$	(%)
pole	$90°$	0	0	0	0.38	0.42	10
polar circle	$90° - \epsilon$	0.38	0.42	10	0.71	0.77	8
middle	$45°$	0.71	0.71	0	0.92	0.94	2
tropical circle	ϵ	0.92	0.91	-1	1	1	0
equator	0	1	1	0	0.92	0.91	-1
tropical circle	$-\epsilon$	0.92	0.91	-1	0.71	0.64	-9
middle	-45	0.71	0.71	0	0.38	0.34	- 10
polar circle	$-90 + \epsilon$	0.38	0.42	10	0	0	0
pole	-90°	0	0	0	0	0	0

the Sun is low above the horizon than when it is high. Finally, it can be shown that the latitudes above the tropical circle of the summer hemisphere receive less energy when ϵ is smaller, which increases the latitudinal contrast, a result also used by Milankovitch (1941) through his caloric insolations to force an ice age. All latitudes south of the tropical circle of the winter hemisphere receive more energy when ϵ decreases.

During the time obliquity is going through a full cycle, precession goes to about 2 cycles. Over each cycle, the precessional factor, $(1 + e \cos v)^2$, changes between two extrema: $(1-e)^2$ and $(1+e)^2$, which are reached respectively for $\lambda - \tilde{\omega} = 180°$ (Earth at the aphelion) and $\lambda - \tilde{\omega} = 0°$ (Earth at the perihelion). For example, we have:

for $\lambda = 0$ ($\delta = 0$) $\tilde{\omega} = 180°$ (autumnal equinox at perihelion)
$\tilde{\omega} = 0°$ (vernal equinox at perihelion)

for $\lambda = 90°$ ($\delta = \epsilon$) $\tilde{\omega} = 270°$ (winter solstice at perihelion)
$\tilde{\omega} = 90°$ (summer solstice at perihelion)

This change between the two extremes of the precessional factor is equal to $4e$. It reaches for e=0, 0.02, 0.04 and 0.075 respectively 0, 8, 16 and 30 %. It must be stressed here that these extrema within the precessional cycle reinforce considerably the spectral power at the eccentricity periods, in particular for those originating from a beat between one of the 23 ka-periods and one of the 19 ka-periods As shown in section 2 of this paper, those

"23-19" combinations lead to beat periods located between 95 and 130 ka contributing to the so-called 100 ka-eccentricity cycle (so-called 100 ka period) because most of the time the lack of resolution does not allow to discriminate between 95 and 130 ka. For the other beats leading to the eccentricity periods numbers 1 and 6 in Table 1, the problem is more complicated because one would have to be able to discriminate between the precessional periods numbers 1 and 2, where the difference amounts only 1300 yr or between numbers 3 and 4 where the difference is less than 200 years. Moreover, the time series would need also to be long enough to detect the 400 ka and 2,300 ka periods).

But, these extrema of the precessional factor are weighted by the eccentricity factor $(1 - e^2)^{-2}$, which means that they become respectively $(1 + e)^{-2}$ and $(1 - e)^{-2}$. They contribute to a change from 1 to 1 (0 %), 0.96 to 1.04 (8 %), 0.92 to 1.09 (17 %) and 0.86 to 1.17 (31 %), for the four eccentricity values just considered. As the long term variation of e is roughly 5 times slower than that of the climatic precession, this eccentricity factor contributes very little to the modulation of the precession factor over one precessional cycle. But over one full eccentricity cycle, $(1 - e^2)^{-2}$ can change W_{Noon} by a maximum of 1 %.

All these comparisons between the relative contribution of ϵ, $e \sin\tilde{\omega}$ and e hold for all latitudes and days for which $W \neq 0$. For any eccentricity value above roughly the present-day value, the precessional term dominates everywhere, but mainly in middle and low latitudes. It is only in high polar latitudes, where W_{Noon} is smaller, that the obliquity plays relatively a more significant role.

These results are difficult to generalise for all hours of the day. The reason lies in $\cos z$ (see 18), $\cos H$ weighting $\cos\delta$ but not $\sin\delta$. Being given the range within which δ is allowed to vary ($-\epsilon \leq \delta \leq \epsilon$), $\cos\delta$ is at least more than twice as large as $\sin\delta$, which according to the value of H will give ϵ more or less power. This will also depend upon the latitudes through the $\sin\phi$ and $\cos\phi$ factors. Finally, the value of $\cos z$ will depend upon the signs of $\sin\phi \sin\delta$ and of $\cos\phi \cos\delta \cos H$, which needs to consider whether or not ϕ and δ have the same sign and $| H |$ is greater than 90^o (6 hours). This can be seen numerically through spectral analysis of the instantaneous insolation values at noon summer solstice for all latitudes (e.g. Figure 9 or other examples in Berger et al., 1993b).

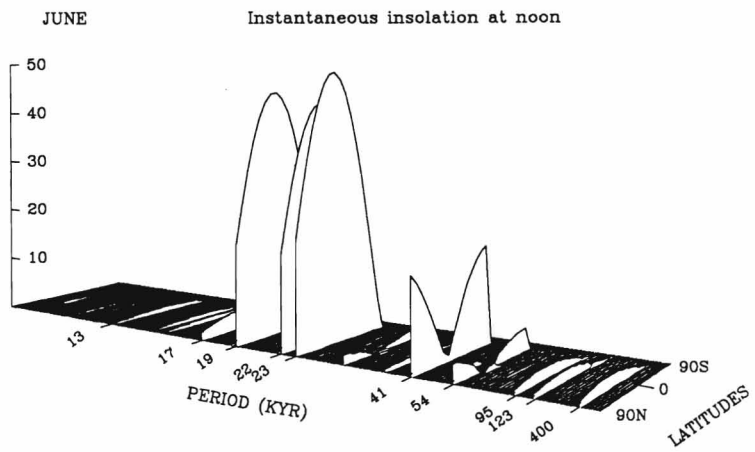

Figure 9: Spectral amplitude in the Thomson multi-taper harmonic analysis of the instantaneous insolation at noon for summer solstice (June) and for each latitude between the north pole and the south pole.

9 Equator, Poles and Equinoxes

Simplifications are occuring in three particular cases related to this instantaneous insolation at a given time t: insolation at the equator W_{EQ}, insolation at the pole W_{PO}, and insolation at the equinoxes (vernal and autumnal) W_{VA}.

At the equinoxes, $\delta = 0$ implies that $H_0 = 90°$ (or 6 hours) for all latitudes as it can be deduced from (36). For the instantaneous insolation, we have:

$$W_{VA} = S_a \left(\frac{a}{r} \right)^2 \cos\phi \, \cos H \tag{44}$$

which shows that whatever the time of the day we consider, W_{VA} does not depend at all of obliquity. It is strictly a function of precession and eccentricity as it can be deduced from a geometrical point of view: at the equinoxes, the axis of rotation of the Earth lies

in a plane normal to the solar beam. The relative importance of the precessional and eccentricity components is the same as already discussed in the previous sections, for any latitude and time of the day.

At the equator, $\phi = 0$ implies that $H_o = 90^o$ (or 6 hours) for all days of the year as it can be deduced from (36). For the instantaneous insolation, we have:

$$W_{EQ} = S_a \left(\frac{a}{r}\right)^2 \cos\delta \cos H \tag{45}$$

Except at the equinoxes, W_{EQ} is therefore a function of ϵ through $\cos\delta$:

$$\cos\delta = \sqrt{1 - \sin^2 \epsilon \sin^2 \lambda}$$

whatever the time of the day we consider. Its maximal influence is felt for $\lambda = 90^o$ or 270^o, it means at the solstices, but remains very weak, as it can be seen from Table 3. At such solstices, the equator receives more energy when ϵ is small, as already concluded from Table 3:

$$W_{EQ} = S_a \left(\frac{a}{r}\right)^2 \cos\epsilon \cos H \tag{46}$$

At the pole, $\phi = 90^o$ and (18), leads to

$$\cos z = \sin\delta$$

which shows that the altitude of the Sun (above the horizon) does not change very much over 24 hours during the long polar day. In such a case, for any instantaneous time during that long day, we have:

$$W_{PO} = S_a \left(\frac{a}{r}\right)^2 \sin\delta = S_a \left(\frac{a}{r}\right)^2 \sin\epsilon \sin\lambda \tag{47}$$

At the poles, there is either :

no sunrise:	$H_o = 0$	if $\phi.\delta \leq 0$
or no sunset:	$H_o = 180^o$ (or 12h)	if $\phi.\delta > 0$

This means that at the northern pole, $W_{PO} \neq 0$ for $0 < \lambda < 180^o$ with a maximum weight of ϵ for $\lambda = 90^o$. At that time, the pole receives less energy when ϵ is small (as shown again in Table 3):

$$W_{PO} = S_a \left(\frac{a}{r}\right)^2 \sin\epsilon \tag{48}$$

(46) and (48) lead clearly to an intensification of the latitudinal gradient of insolation at small ϵ.

10 Total daily insolation

The total daily insolation is simply obtained by integrating (17) over 24 hours of true solar time, t_s. But we must represent the diurnal march of irradiation as a function of the mean solar time, t, which, by definition, is regular, the true solar time being not because of the elliptical shape of the orbit and the second law of Kepler. The relation between the two is given by the equation of time, ET, provided in the Astronomical Ephemeris for each day (see 20)

$$t_s = t + ET$$

Therefore

$$\frac{dt_s}{dt} = 1 + \frac{dET}{dt}$$

and neglecting the small variations of ET compared to 1, we have $dt \sim dt_s$. As the solar hour-angle, H, in time units is called t_s, we have

$$H = \frac{2\pi}{\tau} t_s$$

where τ is the interval of 24 hours. Therefore,

$$dH = \frac{2\pi}{\tau} dt_s \simeq \frac{2\pi}{\tau} dt \tag{49}$$

and assuming r is constant over the day, the integration of (17) becomes:

$$\overline{W}_d = \frac{1}{\tau} \int_{24h} W \, dt = \frac{S_a}{2\pi} \left(\frac{a}{r}\right)^2 \int_{-H_o}^{H_o} \cos z \, dH$$

which gives:

- for the latitudes where there is a daily sunrise and sunset:

$$| \phi | < 90^o - | \delta |$$

$$\overline{W}_d = \frac{S_a}{\pi} \left(\frac{a}{r}\right)^2 (H_o \sin\phi \sin\delta + \cos\phi \cos\delta \sin H_o) \tag{50}$$

$$\text{length of the day} = \frac{24h}{\pi} \cos^{-1} (- \tan \phi \tan \delta)$$

- for the latitudes $| \phi | \geq 90^o - | \delta |$

  - the long polar night is defined by: $\phi.\delta \leq 0$

$$\text{and we have :} \quad \overline{W}_d = 0 \tag{51}$$

$$\text{length of the day} = 0$$

- the long polar day is defined by: $\phi.\delta > 0$

$$\text{and we have :} \quad \overline{W}_d = S_a \left(\frac{a}{r}\right)^2 \sin\phi \sin\delta \qquad (52)$$

$$\text{length of the day} = 24h.$$

This has been discussed in length in Berger (1978). The spectral behaviour of this daily insolation was presented in Berger and Pestiaux (1984) and Berger et al. (1993b). It can be summarized as follows

1. for the equinoxes:

$$\begin{matrix}\text{vernal}\\ \text{autumnal}\end{matrix} \text{ equinox : } \overline{W}_d = \frac{S_a}{\pi} \frac{(1 \pm e \cos\tilde{\omega})^2}{(1-e^2)^2} \cos\phi \qquad (53)$$

   Formula (53) holds for all latitudes.

2. for the solstices:

$$\begin{matrix}\text{summer}\\ \text{winter}\end{matrix} \text{ solstice : } \overline{W}_d = \frac{S_a}{\pi} \frac{(1 \pm e \sin\tilde{\omega})^2}{(1-e^2)^2} (\pm H_o \sin\phi \sin\epsilon + \cos\phi \cos\epsilon \sin H_o) \qquad (54)$$

   with $\cos H_o = \mp \tan\phi \tan\epsilon$ for the daily sunrise and sunset. But formula (54) holds also for the two following particular cases:

   - the long polar night: $|\phi| \geq 90^\circ - \epsilon$, $\phi.\delta \leq 0$: $H_o = 0$

   - the long polar day: $|\phi| \geq 90^\circ - \epsilon$ $\phi.\delta > 0$: $H_o = 180^\circ$

Again we must stress that the numerical value of $\tilde{\omega}$ is "the numerical value obtained from the astronomical serie which development is given in Berger (1978)" plus 180°.

(53) clearly shows that $\overline{W}_d$ at the equinoxes is only a function of precession, as already concluded for the instantaneous insolation W_{VA}. At the solstices, (54) shows that although the ϵ effect is more important at high than at low latitudes, the precession effect still dominates except at the high latitudes of the winter hemisphere (close to the polar circle).

Moreover, just as in the case of instantaneous insolation, for a given time λ in the year, the equation (50) shows that the precession and obliquity signals in the daily insolation originate from two distinct factors: the precession signal arises through

$$(1 + e \cos(\lambda - \tilde{\omega}))^2 \tag{55}$$

in the distance factor and the obliquity signal comes from the factor

$$H_0 \sin\phi \sin\delta + \cos\phi \cos\delta \sin H_0 \tag{56}$$

This characteristic allows to follow more easily the impact of precession and obliquity variations in both hemispheres: the obliquity plays the same role in both hemispheres during the same local season. Indeed equation (56) takes the same value for a latitude ϕ and a time λ in the year (corresponding to δ) than for a latitude $(-\phi)$ and a time $(\lambda + 180^o)$ (corresponding to $-\delta$). On the contrary precession has an opposite effect on both hemispheres. Indeed for a latitude ϕ and a season corresponding to $\lambda(\delta)$ the variation is given by (55). For a latitude $(-\phi)$ and a season corresponding to $(\lambda + 180^o)$ $(-\delta)$, the variation reverses as $e \cos(\lambda - \tilde{\omega})$ in (55) changes its sign and (56) holds.

11 Conclusions

The analytical expressions providing the insolation at given latitude, day of the year and time of the day have confirmed the spectral analysis of the numerical values which can easily be computed through the usual formulas. Some particular dates and times of the day have provided examples which illustrate clearly that in most occasions, the precessional signal dominates the obliquity one, except in high polar latitudes mainly of the winter hemisphere.

Other parameters than the instantaneous and daily insolations can be analysed. These are, for example, irradiation received during some particular times of the day (Cerveny, 1991 and Berger et al., 1993b), or integrated over a specific part of the year and over a given zonal band (Berger, 1975; Godart, 1986; Loutre, 1993). Their spectral behaviour give some interesting information which in addition to the results presented in this paper allow to analyse how the climate system might respond to the insolation forcing. However, as there are many non-linear feedbacks intervening, it is necessary to go well beyond the comparison of the spectra of the insolations (input to the climate system) and of

the geological records (proxy for the output of the system). Climate models, and in particular those which are able to reproduce the transient response of the full climate system to the insolation forcing (e.g. Berger et al., 1990; Gallée et al., 1992) are urgently needed to better understand the mechanisms through which the astronomical frequencies (amplitudes and phases) are transformed.

12 References

Backman J., Pestiaux P., Zimmerman H. and O. Hermelin, 1986. Palaeoclimatic and palaeoceanographic development in the Pliocene North Atlantic: Discoaster accumulation and coarse fraction data. In: C.P. Summerhayes and N.J. Shackleton (eds), *North Atlantic Palaeoceanography*, Geological Society, Special Publ. n° 21, pp. 231-242.

Bard E., Hamelin B., Faribanks R.G. and A. Zindler, 1990. Calibration of the ^{14}C timescale over the past 30,000 years using mass spectrometric U-Th ages from Barbados corals. *Nature*, 345, pp. 405-410.

Barnola J.M., Raynaud D., Korotkevitch Y.S. and C. Lorius, 1987. Vostok ice core: a 160,000 year record of atmospheric CO_2. *Nature*, 329(6138), pp. 408-414.

Benzi R., Parisi G., Sutera A. and A. Vulpiani, 1982. Stochastic resonance in climatic change. *Tellus*, 34, pp. 10-16.

Berger A., 1973. Théorie astronomique des paléoclimats. *Thèse de doctorat*, Faculté des Sciences, Université Catholique de Louvain. Unpublished manuscript.

Berger A., 1975. Astronomical theory of paleoclimates: a cascade of accuracy. *WMO-IAMAP*, Norwich, WMO n° 421, pp. 65-72, Genève.

Berger A., 1976. Obliquity and precession for the last 5,000,000 years. *Astronomy and Astrophysics*, 51, pp. 127-135.

Berger A., 1977a. Support for the astronomical theory of climatic change. *Nature*, 268, pp. 44-45.

Berger A., 1977b. Long term variations of the Earth's orbital elements. *Celestial Mechanics*, 5, pp. 3-74.

Berger A., 1978. Long term variations of daily insolation and Quaternary climatic changes. *Journal of Atmospheric Sciences*, 35(12), pp. 2362-2367.

Berger A., 1988. Milankovitch theory and climate. *Review of Geophysics*, 26(4), pp. 624-657.

Berger A., 1989a. Pleistocene climatic variability at astronomical frequencies. *Quaternary International*, 2, pp. 1-14.

Berger A., 1989b. The spectral characteristics of pre-Quaternary climatic records, an example of the relationship between the astronomical theory and geo-sciences. In: A. Berger, S. Schneider and J.Cl. Duplessy (eds), *Climate and Geo-Sciences, a Challenge for Science and Society in the 21st Century*, pp. 47-76, Kluwer, Dordrecht, Holland.

Berger A. and P. Pestiaux, 1984. Accuracy and stability of the Quaternary terrestrial insolation. In: A. Berger, J. Imbrie, J. Hays, G. Kukla and B. Saltzman (eds), *Milankovitch and Climate*, pp. 83-112, D. Reidel Publ. Company, Dordrecht, Holland.

Berger A., Loutre M.F. and V. Dehant, 1989. Influence of the changing lunar orbit on the astronomical frequencies of pre-Quaternary insolation patterns. *Paleoceanography*, 4(5), pp. 555-564.

Berger A. and M.F. Loutre, 1990. Origine des fréquences des éléments astronomiques intervenant dans le calcul de l'insolation. *Bulletin Sciences*, 1-3/90, pp. 45-106, Académie Royale des Sciences, des Lettres et des Beaux-Arts de Belgique.

Berger A., Gallée H., Fichefet Th., Marsiat I. and C. Tricot, 1990. Testing the astronomical theory with a coupled climate-ice sheet model. In: L.D. Labeyrie and C. Jeandel (eds), Geochemical Variability in the Oceans, Ice and Sediments. *Palaeogeography, Palaeoecology*, 89(1/2), *Global and Planetary Change Section*, 3(1/2), pp. 125-141.

Berger A. and M.F. Loutre, 1991. Insolation values for the climate of the last 10 million years. *Quaternary Science Reviews*, 10 n°4, pp. 297-317.

Berger A., Gallée H. and C. Tricot, 1993a. Glaciation and deglaciation mechanisms in a coupled 2-D climate - ice sheet model. *Journal of Glaciology*, (in press).

Berger A., Loutre M.F., and C. Tricot, 1993b. Insolation and Earth's orbital periods. *J. Geophys. Res.*, (in press).

Birchfield G.E. and J. Weertman, 1978. A note on the spectral response of a model continental ice sheet. *Journal of Geophysical Research*, 83(C8), pp. 4123-4125.

Boyle E.A. and L.D. Keigwin, 1985/1986. Comparison of Atlantic and Pacific paleochemical records for the last 215,000 years: Changes in deep ocean circulation and chemical inventories. *Earth Plan. Sci. Lett.*, 76, pp. 135-150.

Bretagnon P., 1974. Termes à longues périodes dans le système solaire. *Astronomy and Astrophysics*, 30(1), pp. 141-154.

Broecker W.S., Thurber D.L., Goddard J., Ku T., Matthews R.K. and K.J. Mesolella, 1968. Milankovitch hypothesis supported by precise dating of coral reefs and deep sea sediments. *Science*, 159, pp. 297-300.

Brouwer D., and G.M. Clemence, 1961. *Methods of Celestial Mechanics.* Academic Press, New York, 598p.

Cerveny R.S., 1991. Orbital signals in the diurnal cycle of radiation. *J. Geophys. Res.*, 96(D9), pp. 17,209-17,215.

CLIMAP Project Members, 1976. The surface of the Ice-Age Earth. *Science*, 191, pp. 1131-1137.

CLIMAP Project Members, 1981. Seasonal reconstruction of the Earth's surface at the Last Glacial maximum, McIntyre A. and Cline R. (eds), Geological Society of America. Map and Chart Series MC-36, Boulder, pp. 1-18.

COHMAP Members, 1988. Climatic changes of the last 18,000 years: Observations and model simulations. *Science*, 241, pp. 1043-1052.

Crowley T.J., 1988. Paleoclimate modelling. In: M. Schlesinger (ed.), *Physically-Based Modelling and Simulation of Climate and Climatic Change*, pp. 883-949, Kluwer Academic Publishers, Dordrecht, Holland.

Curry W.B. and T.J. Crowley, 1987. The $\delta^{13}C$ of equatorial Atlantic surface waters: implications for ice-age pCO_2 levels. *Paleoceanography*, 2, pp. 489-517.

Emiliani C., 1966. Isotopic paleotemperatures. *Science*, 154(3751), pp. 851-857.

Fischer A.G., 1986. Climatic rhythms recorded in strata. *Ann. Rev. Earth Planet. Sci.*, 14, pp. 351-376.

Gallée H., van Ypersele J.P., Fichefet Th., Marsiat I., Tricot C. and A. Berger, 1992. Simulation of the last glacial cycle by a coupled, sectorially averaged climate - ice-sheet model. II. Response to insolation and CO_2 variation. *Journal of Geophysical Research*, 97(D14), pp. 15,713- 15,740.

Ghil M., and H. Le Treut, 1981. A climate model with Cryodynamics and Geodynamics. *Journal of Geophysical Research*, 86, pp. 5262-5270.

Godart O., 1986. Geometrical insolation of a planet. *Annales de la Société Scientifique de Bruxelles*, T. 100 II, pp. 53-85.

Hasselman K., 1976. Stochastic climate models, part I. *Tellus*, 28, p. 473.

Hays J.D., Imbrie J. and N.J. Shackleton, 1976. Variations in the Earth's orbit: pacemaker of the Ice Ages. *Science*, 194, pp. 1121-1132.

Herbert T.D. and A.G. Fischer, 1986. Milankovitch climatic origin of mid-Cretaceous black shale rhythms, Central Italy. *Nature*, 321(6072), pp. 739-743.

Hilgen F.J., 1987. Sedimentary rhythms and high resolution chrono-stratigraphic correlations in the Mediterranean Pliocene. *Newsletters Stratigraphy*, 17(2), pp. 109-127.

Hilgen F.J. and C.G. Langereis, 1989. Sedimentary cycles in the Mediterranean Pliocene: discrepancies with the quasi-periods of the Earth's orbital cycles ? In: D.G. Smith, A. Berger, P.L. de Boer (eds), *Milankovitch Cyclicity in the Pre-Pleistocene Stratigraphic Record, Terra Abstracts*, 1(1), p. 241.

Hyde W.T. and W.R. Peltier, 1985. Sensitivity experiments with a model of the ice age cycle. The response of harmonic forcing. *Journal of Atmospheric Sciences*, 42(20), pp. 2170-2188.

Imbrie J., and J.Z. Imbrie, 1980. Modelling the climatic response to orbital variations. *Science*, 207, pp. 943-953.

Imbrie J., and N.G. Kipp, 1971. New micropaleontological method for quantitative paleoclimatology: application to a Late Pleistocene Caribbaen Core. In: K.K. Turekian (ed.), *Late Cenozoic Glacial Ages*, pp. 71-81, Yale University Press, New Haven.

Imbrie J., Hays J., Martinson D.G., McIntyre A., Mix A.C., Morley J.J., Pisias N.G., Prell W.L. and N.J. Shackleton, 1984. The orbital theory of Pleistocene climate: support from a revised chronology of the marine ^{18}O record. In: A. Berger, J. Imbrie, J. Hays, G. Kukla and B. Saltzman (eds), *Milankovitch and Climate*, pp. 269-305, D. Reidel Publ. Company, Dordrecht, Holland.

Imbrie J., McIntyre A. and A. Mix, 1989. Oceanic response to orbital forcing in the Late Quaternary: observational and experimental strategies. In: Berger A., Schneider S., and Duplessy J.Cl. (eds), *Climate and Geo-Sciences*, pp. 121-164, Kluwer, Dordrecht, Holland.

Janecek T.R. and D.K. Rea, 1984. Pleistocene fluctuations in Northern Hemisphere tradewinds and westerlies. In: A. Berger, J. Imbrie, J. Hays, G. Kukla and B. Saltzman (eds), *Milankovitch and Climate*, pp. 331-347, D. Reidel, Dordrecht, Holland.

Jouzel J., Lorius Cl., Petit J.R., Genthon C., Barkov N.I. and V.M. Kotlyakov and V.M. Petrov, 1987. Vostok ice core: a continuous isotope temperature record over the last climatic cycle. *Nature*, 329(6138), pp. 403-408.

Kominz M.A. and N.G. Pisias, 1979. Pleistocene climate: deterministic or stochastic? *Science*, 204, pp. 171-173.

Kutzbach J.E., 1985. Modeling of paleoclimates. *Adv. Geophys.*, 28A, pp. 159-196.

Laskar J., 1988. Secular evolution of the solar system over 10 millions years. *Astronomy and Astrophysics*, 198, pp. 341-362.

Lean J., 1991. Variations in the Sun's radiative output. *Review of Geophysics*, 29(4), pp. 505-535.

Lindzen R.S., 1986. A simple model for 100K-year oscillations in glaciation. *Journal of Atmospheric Sciences*, 43(10), pp. 986-996.

Loutre M.F., 1993. Paramètres orbitaux et cycles diurne et saisonnier des insolations. *Thèse de doctorat*, Faculté des Sciences, Université Catholique de Louvain, Louvain-la-Neuve. Unpublished manuscript.

McIntyre A., Ruddiman W.F., Karlin K. and A.C. Mix, 1989. Surface water response of the equatorial Atlantic Ocean to orbital forcing. *Paleoceanography*, 4, pp. 19-55.

Milankovitch M., 1941. *Kanon der Erdbestrahlung.* Royal Serbian Academy, Spec. publ. 132, section of Mathematical and Natural Sciences, vol. 33 (published in English by Israel program for Scientific Translation, for the U.S. Department of Commerce and the National Science Foundation, Washington D.C., 1969).

Molfino B., Heusser L.H. and G.M. Woillard, 1984. Frequency components of a Grande Pile pollen record: Evidence of precessional orbital forcing. In: A. Berger, J. Imbrie, J. Hays, G. Kukla and B. Saltzman (eds), *Milankovitch and Climate*, pp. 391-404, D. Reidel, Dordrecht, Holland.

Negrini R.M., Verosub K.L. and J.O. Davis, 1988. The middle to late Pleistocene geomagnetic field recorded in fine-grained sediments from Summer Lake, Oregon, and Double Hot Springs, Nevada, USA. *Earth and Planetary Science Letters*, 87, pp. 173-192.

Nicolis C., 1980. Response of the Earth-atmosphere system to a fluctuating solar input. In: *Sun and Climate*, pp. 385-396, CNES-CRS-DGRST, Toulouse, October 1980.

Nicolis C., 1982. Stochastic aspects of climatic transitions-response to a periodic forcing. *Tellus*, 34, pp. 1-9.

Oerlemans J., 1980. Model experiments on the 100,000-yr glacial cycle. *Nature*, 287, pp. 430-432.

Olsen P.E., 1986. A 40-million-year lake record of Early Mesozoic orbital climatic forcing. *Science*, 234, pp. 842-848.

Pestiaux P., van der Mersch I., Berger A. and J.Cl. Duplessy, 1988. Paleoclimatic variability at frequencies ranging from 1 cycle per 10,000 years to 1 cycle per 1,000 years: evidence for non-linear behavior of the climate system. *Climatic Change*, 12(1), pp. 9-37.

Pokras E.M. and A.C. Mix, 1987. Earth's precession cycle and Quaternary climatic changes in tropical Africa. *Nature*, 326, pp. 486-487.

Pollard D., 1982. A simple ice sheet model yields realistic 100 kyr glacial cycles. Nature, 296, pp. 334-338.

Pollard D., 1984. Some ice-age aspects of a calving ice-sheet model. In: Berger A., Imbrie J., Hays J., Kukla G. and Saltzman B. (eds), *Milankovitch and Climate*, pp. 541-564, Reidel Dordrecht, Holland.

Prell W.L., 1984. Monsoonal climate of the Arabian Sea during the late Quaternary: A response to changing solar radiation. In: Berger A., Imbrie J., Hays J., Kukla G. and Saltzman B. (eds), *Milankovitch and Climate*, pp. 349-366, Reidel, Dordrecht, Holland.

Ruddiman W.F. and A. McIntyre, 1984. Ice-age thermal response and climatic role of the surface Atlantic Ocean, 40°N to 63°N. *Geol. Soc. Am. Bull.*, 95, pp. 381-396.

Ruddiman W.E., Shackleton N.J. and A. McIntyre, 1986. North Atlantic sea-surface temperatures for the last 1.1 million years. In: Summerhayes C.P. and Shackleton N.J. (eds), *North Atlantic Palaeoceanography Geological Society Special Publication*, 21, pp. 155-173.

Saltzman B., Hansen A.R. and K.A. Maasch, 1984. The Late Quaternary glaciations as the response of a three-component feedback system to earth-orbital forcing. *Journal of Atmospheric Sciences*, 41(23), pp. 3380-3389.

Shackleton N.J. and N.G. Pisias, 1985. Atmospheric carbon dioxide, orbital forcing, and climate. In: E.T. Sundquist and W.S. Broecker (eds), *The Carbon Cycle and Atmospheric CO_2: natural variations Archean to Present*, pp. 303-317, Geophys. Mono. 32. Am. Geophys. Union, Washington D.C.

Shackleton N.J., Imbrie J. and N. Pisias, 1988. The evolution of oceanic oxygen-isotope variability in the North Atlantic over the past three million years. *Phil. Trans. R. Soc. London*, B318, pp. 679-688.

Shackleton N.J., Berger A. and W.R. Peltier, 1990. An alternative astronomical calibration of the lower Pleistocene timescale based on ODP site 677. *Transactions of the Royal Society of Edinburgh: Earth Sciences*, 81, pp. 251-261.

Short D.A., Mengel J.G., Crowley T.J., Hyde W.T. and G.R. North, 1991. Filtering of Milankovitch cycles by Earth's geography. *Quaternary Research*, 35, pp. 157-173.

Stothers R.B., 1987. Do slow orbital periodicities appear in the record of Earth's magnetic reversals ? *Geophysical Research Letters*, 14(11), pp. 1087-1090.

Weedon G.P., 1985/1986. Hemipelagic shelf sedimentation and climatic cycles: the basal Jurassic (Blue Lias) of South Britain. *Earth and Planetary Science Letters*, 76, pp. 321-335.

Wigley T.M.L., 1976. Spectral analysis: astronomical theory of climatic change. *Nature*, 264, pp. 629-631.

Woillard G.M., 1978. Grande Pile peat bog: A continuous pollen record for the last 140,000 years. *Quaternary Research*, 9, pp. 1-21.

Woolard E.W. and G.M. Clemence, 1966. *Spherical Astronomy.* Academic Press, New York, London.

Yiou P., Genthon C., Ghil M., Jouzel J., Le Treut H., Barnola J.M., Lorius Cl. and Y.N. Korotkevitch, 1991. High-frequency paleovariability in climate and CO_2 levels from Vostok ice-core records. *Journal of Geophysical Research*, 96 n° B12, pp. 20,365-20,378.

ANNEX 1 - Arithmetic mean of r

Let us calculate the mean value of the Earth-Sun distance over one year:

$$< r > = \frac{1}{T} \int_0^T r \, dt$$

If we introduce the eccentric anomaly, E, we have

$$r = a(1 - e \cos E)$$

E is an angle which varies with v and is used in the parametric equation of the ellipse (Brouwer and Clemence, 1961):

$$dv = \frac{a}{r}\sqrt{1 - e^2} \, dE$$

and

$$\frac{dE}{dt} = \frac{2\pi}{T} \frac{a}{r}$$

which leads to:

$$< r > = \frac{a}{2\pi} \int_0^{2\pi} (1 - e \cos E)^2 = a\left(1 + \frac{e^2}{2}\right)$$

to compare with $r_m = a(1 - e^2)^{\frac{1}{4}} \sim a(1 - \frac{e^2}{4})$. As an example for $e = 0.02$, $< r > = 1.0002 \; a$ and $r_m = 0.9999 \; a$. Energetically speaking the weighted averaged value of r is smaller than a, whereas the arithmetic mean is larger than a.

ANNEX 2

Length of the seasons.

It might be interesting to look for the position of the solstices and autumn equinox relative to a spring equinox arbitrarily fixed at March 21, for example. This might be done from the relationship between the real Sun and the mean Sun and the definition of the equinoxes and solstices. If λ is the longitude of the true Sun along the ecliptic, this longitude being measured counterclockwise from the vernal equinox, we have:

$$\sin\delta = \sin\lambda \sin\varepsilon$$

and the beginning of the astronomical seasons defined relative to the northern hemisphere is given by:

$$\lambda = 0 \quad \text{for} \quad \text{spring}$$
$$\lambda = 90^o \quad \text{for} \quad \text{summer}$$
$$\lambda = 180^o \quad \text{for} \quad \text{autumn}$$
$$\lambda = 270^o \quad \text{for} \quad \text{winter}$$

If λ_m is the longitude of the mean Sun, we have (Brouwer and Clemence, 1961; Berger, 1978):

$$\lambda_m = \lambda - 2\left[\beta(1+\cos\varphi)\sin v - \beta^2(\frac{1}{2}+\cos\varphi)\sin 2v + \beta^3(\frac{1}{3}+\cos\varphi)\sin 3v - ...\right] \quad (1)$$

and

$$\begin{aligned}\lambda = \lambda_m \; &+ \left(2e - \frac{1}{4}e^3 + \frac{5}{96}e^5 + \frac{107}{4608}e^7\right)\sin M \\ &+ \left(\frac{5}{4}e^2 + \frac{11}{24}e^4 + \frac{17}{192}e^6\right)\sin 2M \\ &+ \left(\frac{13}{12}e^3 + \frac{43}{64}e^5 + \frac{95}{512}e^7\right)\sin 3M \\ &+ \; ... \end{aligned} \quad (2)$$

with v and M being the true and the mean anomalies of the Sun, and

$$\begin{aligned}\cos\varphi &= \sqrt{1-e^2} \\ \beta &= \frac{1}{e}\left(1-\sqrt{1-e^2}\right)\end{aligned}$$

The mean solar longitude λ_m, is computed from (1) for the spring equinox ($\lambda = 0$) arbitrarily fixed at March 21; λ_m can then be calculated for each calendar day defined from an increment of the mean longitude given by $\Delta\lambda_m = \frac{360^o}{365}$, the length of the year being assumed to be 365 mean solar days. From these successive fixed values of λ_m, λ can be computed from (2) to allow the computation of the insolation for that particular calendar day. It must be noted that there is a drift artificially created by introducing the calendar day instead of the theoretical solar day defined by the longitude, λ, of the true Sun. This can be seen when comparing Figure A.2.1 showing the daily irradiation computed at the autumn equinox (September) and Figure A.2.2 showing the daily irradiation computed at September 21. This drift is due to the fact that, at that fixed calendar date, the Earth is not occupying the same position relative to the Sun for different times of the past. 114 kyr ago, September 21, was corresponding to $\lambda = 174^o$; 103 kyrs ago it was corresponding to $\lambda = 189^o$; presently, it is 178^o.Considering a given λ instead of a given λ_m insures that identical physical situations are intercompared through geological times as far as the position of the Earth relative to the Sun is concerned. Unfortunately, it is either true that *a given interval $\Delta\lambda$ will not correspond to the same absolute time length at the different* point of the Earth's orbit (due to second law of Kepler), a problem solved by considering λ_m instead.

On the other hand, for each particular value of λ defining the equinoxes and the solstices, λ_m can be computed from (1). Therefore, from a increment, $\Delta\lambda_m = \frac{360^o}{365}$, it is possible to compute the calendar day which corresponds to the autumn equinox (September) and to the solstices for any time of the past and of the future, or equivalently the length of the astronomical seasons (see Table 2 and Figure A.2.3).

These lengths are totally related to precession as it is confirmed by their hereafter analytical expression. Indeed the second law of Kepler tells us that the area swept over by the line joining the Sun and a planet is proportional to the time elapsed. If T_1 and T_2 are the time elapsed while the radius vector is sweeping over the area A_1 and A_2 respectively, we have

$$T_1 = \frac{A_1}{A_2} T_2$$

Let us now consider the particular case of the astronomical seasons (defined as hereover):

$$A_{\text{year}} = \frac{1}{2} \int_{v=-\tilde{\omega}}^{v=2\pi-\tilde{\omega}} a^2 \rho^2 dv$$

$$A_{\text{spring}} = \frac{1}{2} \int_{v=-\tilde{\omega}}^{v=\pi/2-\tilde{\omega}} a^2 \rho^2 dv$$

$$
\begin{aligned}
A_{\text{summer}} &= \frac{1}{2}\int_{v=\pi/2-\tilde{\omega}}^{v=\pi-\tilde{\omega}} a^2\rho^2 dv \\
A_{\text{autumn}} &= \frac{1}{2}\int_{v=\pi-\tilde{\omega}}^{v=3\pi/2-\tilde{\omega}} a^2\rho^2 dv \\
A_{\text{winter}} &= \frac{1}{2}\int_{v=3\pi/2-\tilde{\omega}}^{v=2\pi-\tilde{\omega}} a^2\rho^2 dv
\end{aligned}
$$

Neglecting the terms in e^2 and higher in ρ^2, the length of the seasons is finally given by:

$$
\begin{aligned}
T_{spring} &\cong \frac{T}{4}\left(1 - \frac{4e}{\pi}(\sin\tilde{\omega} + \cos\tilde{\omega}\right) \\
T_{summer} &\cong \frac{T}{4}\left(1 - \frac{4e}{\pi}(\sin\tilde{\omega} - \cos\tilde{\omega})\right) \\
T_{autumn} &\cong \frac{T}{4}\left(1 + \frac{4e}{\pi}(\sin\tilde{\omega} + \cos\tilde{\omega})\right) \\
T_{winter} &\cong \frac{T}{4}\left(1 + \frac{4e}{\pi}(\sin\tilde{\omega} - \cos\tilde{\omega})\right)
\end{aligned}
$$

where T is the length of the year. This clearly shows that the length of the astronomical seasons are only a function of the climatic precession.

For the "half-year" astronomical seasons of the northern hemisphere, we can therefore write:

$$
\begin{aligned}
T_{summer} &= \frac{T}{2}\left(1 - \frac{4e\,\sin\tilde{\omega}}{\pi}\right) \\
T_{winter} &= \frac{T}{2}\left(1 + \frac{4e\,\sin\tilde{\omega}}{\pi}\right)
\end{aligned}
$$

if $0 \leq \tilde{\omega} \leq 180^o$, the half-year northern hemisphere, summer is shorter than winter and longer for $180^o < \tilde{\omega} < 360^o$.

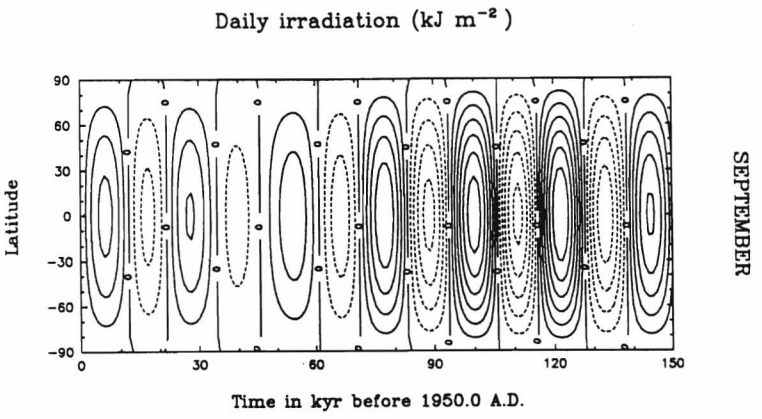

Figure A.2.1: Long term variation of the deviation from present day values for Autumn equinox (September) of the daily irradiation (kJ m^{-2}), contour interval 500 kJ m^{-2}. Solid lines are positive and dashed lines are negative deviations.

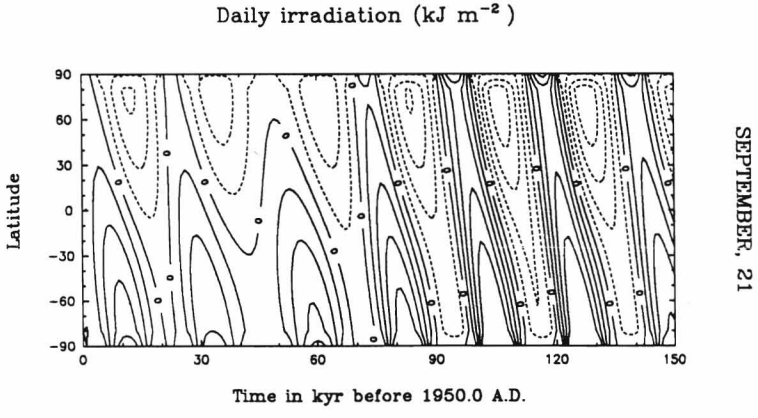

Figure A.2.2: Long term variation of the deviation from present day values for calendar day September 21 of the daily irradiation (kJ m^{-2}), contour interval 1000 kJ m^{-2}. Solid lines are positive and dashed lines are negative deviations.

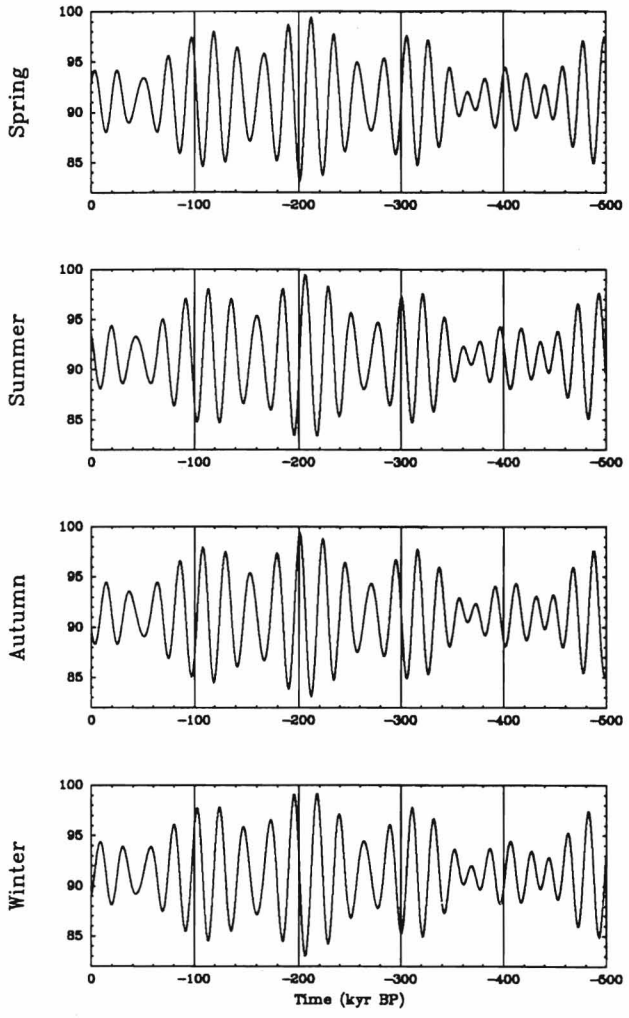

Figure A.2.3: Long-term variations of the length of the seasons over the last 500 kyr; from top to bottom: spring, summer, autumn, winter.